

# **An Improved Method of Cutting Forces Prediction for the Primary Cutting Edges of Twist Drills**

**Igor Minukhin**

A Thesis

in

the Department

of

Mechanical and Industrial Engineering

Presented in Partial Fulfillment of the Requirements

for the Degree of Master of Applied Science (Mechanical Engineering) at

Concordia University

Montreal, Quebec, Canada

March 2013

© IGOR MINUKHIN, 2013

**CONCORDIA UNIVERSITY**

**SCHOOL OF GRADUATE STUDIES**

This is to certify that the Thesis prepared,

By: **Igor Minukhin**

Entitled: **“An Improved Method of Cutting Forces Prediction for the Primary Cutting Edges of Twist Drills”**

and submitted in partial fulfillment of the requirements for the Degree of

**Master of Applied Science (Mechanical Engineering)**

complies with the regulations of the University and meets the accepted standards with respect to originality and quality.

Signed by the Final Examining Committee:

\_\_\_\_\_ Chair  
Dr. W-F. Xie

\_\_\_\_\_ Examiner  
Dr. Y. Zhang

\_\_\_\_\_ External Examiner  
Dr. Z.W. Tian  
Concordia Institute for Information Systems Engineering

\_\_\_\_\_ Supervisor  
Dr. C.Z. Chen

Approved by: \_\_\_\_\_  
Dr. S. Narayanswamy, MASc Program Director  
Department of Mechanical and Industrial Engineering

Date: \_\_\_\_\_

\_\_\_\_\_  
Dean Robin Drew  
Faculty of Engineering & Computer Science

## **ABSTRACT**

This thesis originally proposes an improved theoretical method to predict thrust and torque of twist drills in high speed drilling. The three existing models and methods are thoroughly studied and evaluated. It has been observed that each method has its own advantages as well as drawbacks and some errors.

A fundamental geometrical analysis is carried out on the primary cutting edge of a twist drill to understand the correlation between the geometrical features of the drill and the distribution of cutting forces. The improved method is based on the representation of the cutting forces along the cutting edge as a series of oblique cutting elements. The elemental forces are then integrated to determine the overall thrust force and drilling torque in terms of the basic geometrical features of the drill, the cutting conditions and the properties of the machined material.

The improved method presents the proper definitions of the dynamic rake angle and the uncut chip thickness, proves the negligibility of the feed angle and gives accurate representation of the elemental forces acting along the primary cutting edge, as well as the total thrust force and the torque. A good agreement between the predicted and the experimentally measured forces and torques was found for low carbon steels.

## ACKNOWLEDGEMENT

I would like to dedicate my thesis to the Department of Mechanical and Industrial Engineering, Concordia University.

I would like to sincerely thank my supervisor **Dr. Chevy Chen**, Department of Mechanical & Industrial engineering, Concordia University, for his ongoing support throughout these past three years, for his understanding and continued encouragement and for always having believed that I could contribute to the knowledge and innovation of the Department.

## Table of Contents

List of Figures.....	vii
Chapter 1. Introduction	9
Chapter 2. The cutting forces prediction models and methods	18
2.1 The cutting forces prediction model and the method I [36].....	18
2.1.1 Geometrical model I and relationships .....	18
2.1.2 The force and torque prediction model I .....	21
2.2 The cutting forces prediction model and the method II [34].....	23
2.2.1 Geometrical model II and relationships .....	23
2.2.2 The force and torque prediction model II.....	25
2.3 The cutting forces prediction model and the method III [20].....	27
2.3.1 Geometrical model III and relationships .....	28
2.3.2 The force and torque prediction model III.....	30
2.4 Critical notes and discussion .....	34
Chapter 3. An improved method of cutting forces prediction	45
3.1 Notations .....	45
3.2 Derivation of improved formulas to predict total thrust and torque for the primary cutting edges .....	48

Chapter 4. Applications	64
Chapter 5. Summary and conclusions	76
References	77

## **List of Figures**

Figure1.1. The cutting edges of a standard twist drill. ....	10
Figure1.2. Various shapes of twist drills. ....	16
Figure 2.1. Dynamic geometry of the primary cutting edge by Chen. ....	19
Figure 2.2 Force prediction model by Chen. ....	22
Figure 2.3. Dynamic geometry of the primary cutting edge by Elhachimi. ....	24
Figure 2.4. Force prediction model by Elhachimi. ....	26
Figure 2.5. Dynamic geometry of the primary cutting edge by Armarego. ....	29
Figure 2.6. Force prediction model by Armarego. ....	31
Figure 2.7. Parametrical model for the static rake angle derivation. ....	35
Figure 2.8. Uncut chip thickness. ....	40
Figure 2.9. The distribution of the dynamic, static and feed angles along the cutting edge. ....	41
Figure 2.10. Oxley orthogonal chip formation model. ....	42
Figure 3.1. Oxley oblique cutting model. ....	48
Figure 3.2. The projections of the elemental forces. ....	49
Figure 3.3. The model for force prediction along the primary cutting edge. ....	50
Figure 3.4. Orthogonal chip formation model for force prediction along the primary cutting edge. ....	53
Figure 3.5. Distribution of the various angles along the primary cutting edge on 8 mm standard twist drill. ....	60
Figure 4.1. Comparison of predicted thrust forces for 8 mm standard twist drill. ....	64
Figure 4.2. Comparison of predicted torques for 8 mm standard twist drill. ....	65

Figure 4.3. Prediction of thrust forces using ThirdWave simulation. ....	66
Figure 4.4. Percentage of the total thrust forces and torques acting on the primary cutting edge and chisel edges for different types of twist drills. ....	67
Figure 4.5. Comparison of predicted and experimental thrust forces based on test of Strenkowski. ....	68
Figure 4.6. Comparison of predicted and experimental thrust forces and torques, based on test of Xiong. ....	69
Figure 4.7. Predicted thrust forces for the standard 8, 12 and 16 mm twist drills. ....	70
Figure 4.8. Predicted torques for the standard 8, 12 and 16 mm twist drills. ....	70
Figure 4.9. Predicted trust forces for the standard 8mm twist drill with the 118°, 135° and 140° point angles. ....	71
Figure 4.10. Predicted torques for the standard 8mm twist drill with the 118°, 135° and 140° point angles. ....	72
Figure 4.11. Predicted trust forces for the standard 8mm twist drill with the 30°, 35° and 40° helix angles. ....	72
Figure 4.12. Predicted torques for the standard 8mm twist drill with the 30°, 35° and 40° helix angles. ....	73
Figure 4.13. Predicted thrust forces for the standard 8mm twist drill with the half-web thickness represents 8.5%, 10.5% and 12.5% of the drill radius. ....	74
Figure 4.14. Predicted torques for the standard 8mm twist drill with the half-web thickness represents 8.5%, 10.5% and 12.5% of the drill radius. ....	74

## Chapter 1. Introduction

The importance of drilling in the field of modern metal cutting is based on the fact that drilling is the most common of machining operations performed. The most popular tool is the twist drill, which was invented by Steven A. Morse in 1863 [1], who patented a new drill design, with two spiral flutes and a pointed cutting part, which exceptionally improved the cutting action and chip disposal. The modern twist drill geometry, though similar in the general appearance to the Morse drill, has been the subject of numerous improvements. Usually, a twist drill consists of two main cutting edges; the chisel edge and the cutting lips, as can be seen on Figure 1.1. Some drills have a secondary cutting edge, which significantly reduces the thrust forces and produces a cutting edge with a positive rake and a chip breaking point. The chisel edge protrudes into the workpiece material and contributes mostly to the thrust force. The cutting lips cut out the material and provide the majority of the drilling torque and thrust. During the drilling process, the chips are formed on the cutting edge and moved up along the drill helix angle. The drill geometry has a complicated effect on the cutting forces. A typical twist drill has several design parameters affecting the cutting forces and torque. In fact, the rake angle, inclination angle and the cutting velocity vary along the drill radius. The normal rake angle has a high negative value at the center of the drill, resulting in larger thrust forces and changes from negative to positive along the cutting lips affecting primarily the torque.

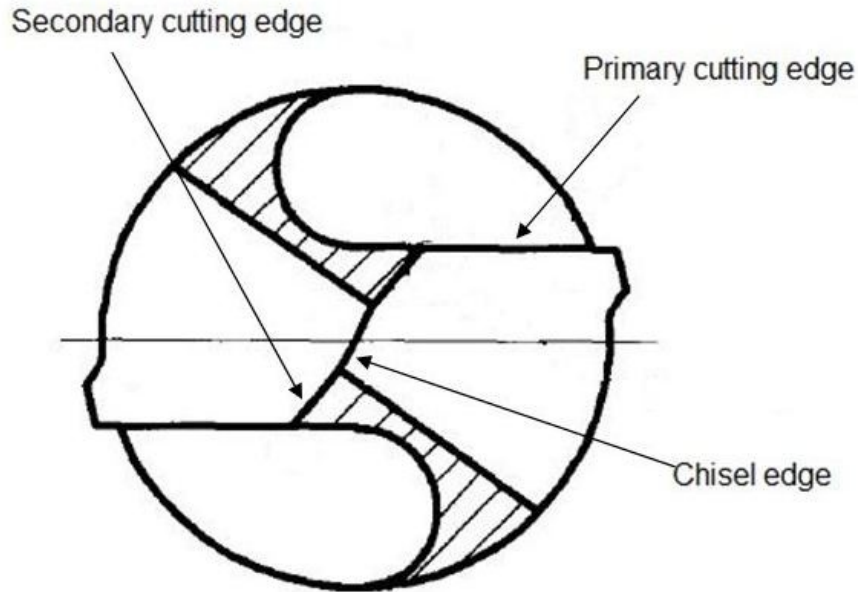


Figure 1.1. The cutting edges of a standard twist drill.

Several simplified models of conducting a metal cutting process analysis have been developed and implemented throughout the past decades. The basic model is called the single-shear plane model or the Ernst-Merchant [2] model, widely presented in most textbooks [3-8]. Based on the principle of energy conservation, Merchant showed that the cutting forces are proportional to the uncut chip area or the chip load. Another model is the theory of Lee and Shaffer [9], who also attempted to solve the metal cutting problems applying the plasticity factor. Both models have numerous drawbacks and disagreements with their respective experimental results. Later on, Hill [10], with his static equilibrium model tried to solve this same problem, stating that the velocity is tangentially discontinuous across the shear plane. Dewhurst [11] also

offered his model of chip formation for the first time analyzing the stress and velocity of boundary conditions.

None of these theories is flawless; and some have been very heavily criticized. However, the simplified analyses predict many of the forces and stresses in the cutting process, including the drilling. In the past years, researchers developed many analytical and numerical models to predict the torque and thrust force in drilling needed to address important process-optimization issues such as the most appropriate and efficient cutting parameters or tool geometries.

Oxford [12] identified a small region all around the middle part of the drill (indentation zone) where the material is not cut but extruded. Outside the indentation zone, the chisel edge performs an orthogonal cut with a negative rake angle. Bera and Bhattacharya [13] analyzed the drill geometry and determined that the chisel edge acted as an indenting tool and the lip as a cutting tool and presented the first predictive cutting model to evaluate the torque and thrust in drilling. They applied the Merchant thin shear zone cutting model to predict the drilling forces at the cutting edge. The total thrust and torque were found by the summation of the elemental thrusts and torques derived from the elemental deformation forces and the thrust and torque components. Williams [14] went further and described the secondary cutting edges along with the main cutting edges and an indentation zone around the drill center as the three identifiable zones of interest. Williams used an orthogonal cutting analysis to model the thrust and torque at the drill cutting edge. The total forces were calculated by the summation of the force generated by the cutting edge and chisel edge as well as the indentation zone.

The difference of his model from the model of Bera and Bhattacharyya was that the cutting action for most of the chisel edge was presented as a classical orthogonal cutting action with continuous chip formation and highly negative rake angles.

Mauch and Lauderbaugh [15], in their model also divided the drill into three regions and implemented the idea of using different cutting processes for each zone. Both the orthogonal and the oblique cutting models were applied to the two elements of the chisel edge and to the main cutting edge area accordingly. They also split the main cutting edge into N elements and calculated the total torque and thrust by summarizing the part values generated in each of these regions.

Armarego and Wright [16] analyzed the fundamental machining data such as shear stress and chip length and the cutting mechanisms of the cutting edge and chisel edge developed a model which can be used to estimate thrust and torque for the different drill flank configurations. They found similarities in the effects of feed rates, spindle speeds and the geometrical characteristics of the drill on the resulting torque and thrust values, regardless of the drill flank configurations used. Armarego and Cheng [17, 18] proposed a new simplified method to predict thrust and torque during drilling for conventional and modified drills. The method of calculation was also based on the implementation of the orthogonal cutting model and the oblique cutting model. Later Wiriyacosol and Armarego [19] further developed this method by implementing an already known principle of dividing the cutting edges into a limited number of cutting elements, which were assumed to be oblique cutting edges on the primary cutting edge and the orthogonal cutting edges on the chisel edge. This method was described

extensively in Armarego's latest textbook [20]. However, the calculations were based on empirical equations provided by the orthogonal cutting tests.

Stephenson and Agapiou [21] developed a static force model for drills with various geometrical parameters. They did not include the effect of the chisel edge in their model, but like other researchers, they focused on the primary cutting edge and split it into small segments. This model was based on calculating the radial forces generated by the drill asymmetries and was developed for the drills with different geometrical shapes. Stephenson and Agapiou represented each elementary force as the product of a specific pressure and chip area, where the specific cutting force coefficients could be found based on simple turning tests and also included in their calculations a hardness correction function to compensate the variation in hardness of the workpiece material.

All of the above mentioned methods identified and pointed out the significant problem in determining the empirical equations for the various cutting parameters. Chandrasekharan et al. [22] suggested a new approach in predicting the cutting forces for drilling based on the geometric similarity of the drills. In their model the force and torque equations were represented in a normalized radial coordinate system. Their model consisted of two main points of interest: the primary cutting edge and the chisel edge. In order to describe the cutting forces on the primary cutting edges they used the Merchant's model and the calculations for the chisel edge were based on the slip line field method derived by Kachanov [23]. They developed a calibration algorithm to extract the cutting model coefficients and implemented the mechanistic force approach to develop the models for the cutting force system.

Later on, many researchers found similarities in the drilling and the oblique cutting processes. Watson [24-27] also applied the oblique machining theories to drilling by dividing the cutting edges of the drill into small segments, performing calculations for each segment, and summing the results. The Watson cutting force model for the chisel edge was based on the classical orthogonal cutting analysis and included the drilling tests to determine the contribution of the chisel edge to the overall torque and thrust. However, the correlation between the predicted values and the experimental results for the whole drill was not as good as the correlation between the experimental and the predicted results for the cutting edge alone. Rubenstein [28, 29] thoroughly investigated the oblique cutting process and derived the expressions for the torque and thrust forces, assuming that the removal process is quasi-orthogonal, but for the drill point it was only sufficient when the drill diameter was large enough in relation to the chisel edge length. Zhang et al. [30] noticed the effect of vibrations and developed his model based on the mechanics of vibrations and the continuous distribution of thrust and torque along the cutting edge and the chisel edge of the twist drill. Wang et al. [31, 32] concluded that vibration drilling is different from conventional drilling and presented a method which involved the development of a dynamic uncut chip thickness for each cutting element at the cutting edge and chisel edge. Their model described the dynamic cutting process, where the mean thrust and torque increased as feed increased under constant vibration. Yang et al. [33] studied the drilling and reaming processes and proposed a dynamic model which included a representation of the forces generated on the cutting edge, the influence of the chisel

edge, the relationship between the machine vibrations and forces and the dynamic machine tool model.

Elhachimi et al. [34, 35], based on the oblique cutting model for the primary cutting edge and the orthogonal cutting model for the chisel edge presented a new theoretical model to predict thrust and torque in high speed drilling. In this model, thrust and torque were calculated in terms of the geometric features of the drill, the cutting conditions and the properties of the machined material. Chen et al. [36] modified the existing force model for the split-point, incorporating the splitting parameters on the secondary cutting edge for predicting the thrust forces and torque. By minimizing the thrust forces and torque, they obtained the optimization of the split-point drill geometry. Kapoor, Chandrasekharan et al. [37-39], Gong and Ehmann et al [40-42] developed various mechanistic drilling models. Other recent developments in drilling models have utilized the finite element method. Fuh [43] explored the use of the finite element method for drilling. Guo and Dornfeld [44] and Min et al. [45] applied the finite element technique for modeling drilling and exit burr formation. Shatla and Altan [46] using the same approach determined the drilling torque and thrust force. Bono and Ni [47, 48] predicted the drill heat flux, temperatures, and the thermal distortion of the drill holes.

Strenkowski et al. [49] developed an analytical finite element technique for predicting the thrust force and torque in drilling with twist drills. The approach was based on representing the cutting forces along the cutting edge as a series of oblique sections and cutting in the chisel region was treated as an orthogonal cutting with different cutting speeds depending on the radial location. An Eulerian finite element

model was used for each section to simulate the cutting forces. The section forces were then combined to determine the overall thrust force and drilling torque. An extension of the technique for predicting drill temperatures has also been described.

Zhao et al. [50] applied the finite element method (FEM) to twist drill stress analysis not for design but for verification. Additional studies on the dynamics of drilling can be found in the various articles of other researchers [51-76].

● Cutting Edge Shapes

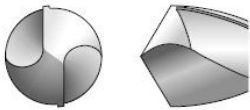
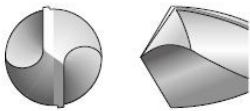
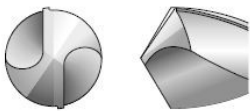
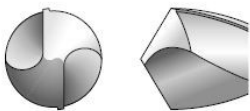
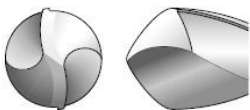
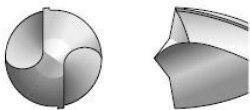
Grinding name	Shape	Features and effect	Application
Conical		<ul style="list-style-type: none"> <li>The flank is conical and the clearance angle increases toward the centre of the drill.</li> </ul>	<ul style="list-style-type: none"> <li>General Use</li> </ul>
Flat		<ul style="list-style-type: none"> <li>The flank is flat.</li> <li>Easy grinding.</li> </ul>	<ul style="list-style-type: none"> <li>Mainly for small diameter drills.</li> </ul>
Three flank angles		<ul style="list-style-type: none"> <li>As there is no chisel edge, the results are high centripetal force and small hole oversize.</li> <li>Requires a special grinding machine.</li> <li>Surface grinding of three sides.</li> </ul>	<ul style="list-style-type: none"> <li>For drilling operations that require high hole accuracy and positioning accuracy.</li> </ul>
Spiral point		<ul style="list-style-type: none"> <li>To increase the clearance angle near the centre of the drill, conical grinding combined with irregular helix.</li> <li>S type chisel edge with high centripetal force and machining accuracy.</li> </ul>	<ul style="list-style-type: none"> <li>For drilling that requires high accuracy.</li> </ul>
Radial lip		<ul style="list-style-type: none"> <li>The cutting edge is ground radial with the aim of dispersing load.</li> <li>High machining accuracy and finished surface roughness.</li> <li>For through holes, small burrs on the base.</li> <li>Requires a special grinding machine.</li> </ul>	<ul style="list-style-type: none"> <li>Cast Iron, Aluminium Alloy</li> <li>For cast iron plates.</li> <li>Steel</li> </ul>
Centre Point drill		<ul style="list-style-type: none"> <li>This geometry has two-stage point angle for better concentricity and a reduction in shock when exiting the workpiece.</li> </ul>	<ul style="list-style-type: none"> <li>For thin sheet drilling.</li> </ul>

Figure 1.2. Various shapes of twist drills (property of Mitsubishi [80])

During the drilling process, it can be observed that due to the various velocities, each segment of the primary cutting edge which lies on the different radial distances

from the drill axis are affected by the different forces. The unequal forces along the cutting edge are causing the different type of the wear: from the chipping and build up edge close to the center area to the extensive wearing and even burning on the peripheral area. This is why researchers and manufacturers are trying to create cutting edge geometries which will be most suitable for the various specific applications. Some examples of the various types of the drill geometries, which contain not only various point angles, rake angle and spiral angles, but also different shapes of flank faces, different chisels as well as primary and secondary cutting edges in case of a split-point drill are shown on Figure 1.2.

## **Chapter 2. The cutting forces prediction models and methods**

In the presented research three models and methods are studied and evaluated.

All three reviewed methods contain two basic steps. First, the authors have determined the geometrical relationships between the various angles. Second, they constructed the force model to predict the cutting forces and torque. Some of the authors have provided the experimental data for the approval of their methods.

### **2.1 The cutting forces prediction model and method I**

#### **2.1.1 Geometrical model I and relationships**

In this work, the authors identify three different regions of interest (the primary cutting edge, the secondary cutting edge and the chisel edge) and then estimate the thrust forces and torque for each of the regions. The geometrical model is shown on Figure 2.1. Based on the authors' opinions, the feed angle must be considered and included into the calculations in each of the three regions.

For any given point on the primary cutting edge the shear angle of the oblique cutting  $\phi$  can be calculated as [28]

$$\cot \phi = \cot \phi_n \cos i - \tan \gamma_d (1 - \cos i) \quad (1)$$

where  $\phi_n$  is the shear angle of the orthogonal cutting,  $i$  is the inclination angle and  $\gamma_d$  is the dynamic rake angle

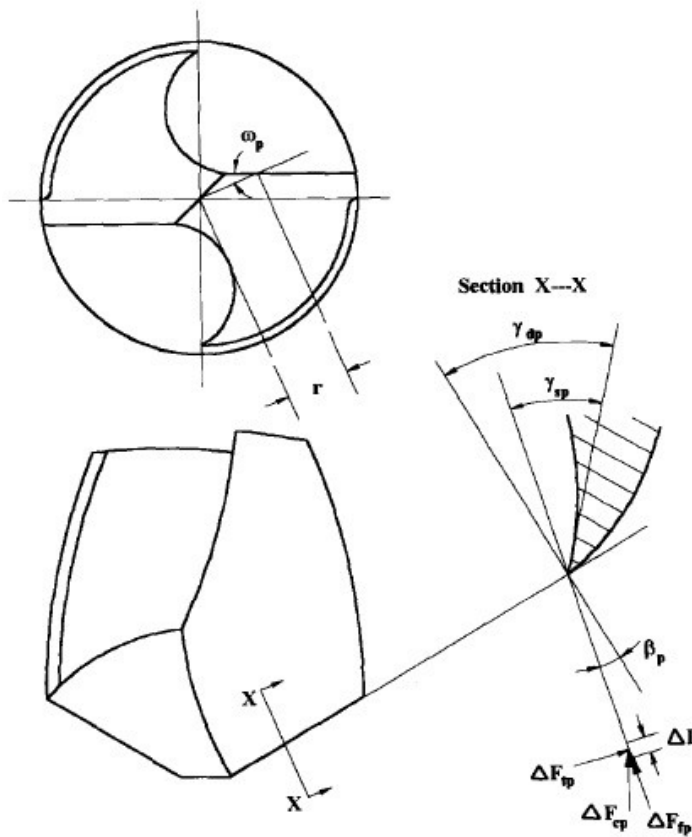


Figure 2.1. Dynamic geometry of the primary cutting edge by Chen.

The shear angle of the orthogonal cutting  $\phi_n$  can be calculated as [2]

$$\phi_n = \frac{\pi}{4} + \frac{\gamma_d - \lambda_n}{2} \quad (2)$$

where  $\lambda_n$  is the friction angle of the orthogonal cutting and may be determined as [77]

$$\lambda_n = \frac{\pi}{6} + \frac{\gamma_d}{2} \quad (3)$$

The inclination angle may be found from the following equation:

$$\sin i = \sin \omega \sin \rho \quad (4)$$

where  $\rho$  is the half-point angle and  $\omega$  is the web angle at a specified radius

Web angle  $\omega$  is given as:

$$\omega = \sin^{-1} \frac{t_p}{r} \quad (5)$$

where  $t_p$  is the half web thickness after the splitting point and  $r$  is the radial distance from the drill axis.

The dynamic rake angle  $\gamma_d$  by the authors' opinions has to be calculated as

$$\gamma_d = \gamma_s + \beta \quad (6)$$

where  $\gamma_s$  is the static rake angle and  $\beta$  is the feed angle

The static rake angle which will be re-considered later, is calculated as

$$\tan \gamma_s = \frac{\tan \delta_r \cos \omega}{\sin \rho - \tan \delta_r \sin \omega \cos \rho} \quad (7)$$

where the helix angle  $\delta_r$  at a specified radius  $r$  and can be found as

$$\tan \delta_r = \frac{r}{R} \tan \delta \quad (8)$$

where  $R$  is the radius of the drill and  $\delta$  is the helix angle at this radius, which are taken from the drill specifications.

Since

$$\text{The tangential velocity} \quad V = 2\pi Nr \quad (9)$$

$$\text{and the axial feed velocity} \quad V_f = fN \quad (10)$$

Feed angle  $\beta$  is calculated as

$$\tan \beta = \frac{f}{2\pi r} \quad (11)$$

where  $f$  is the feedrate

and  $N$  is the drill revolutions.

And finally the friction angle  $\lambda$  can be calculated as [14]

$$\tan(\lambda - \gamma_d) = \frac{\cos \phi - \cos \phi_n + \tan(\lambda_n - \gamma_d) \sin \phi_n}{\sin \phi} \quad (12)$$

### 2.1.2. The force and torque prediction model I

The force and torque prediction model based on the Oxley oblique cutting model [79], which defines the differential force and torque elements for each differential element of the cutting edge.

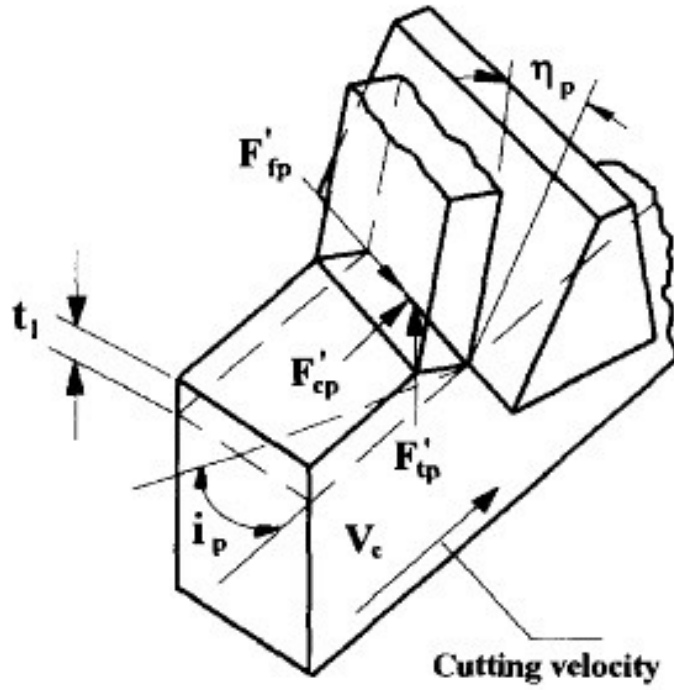


Figure 2.2 Force prediction model by Chen.

The force element in the direction is parallel to the cutting velocity

$$dF_C = \frac{f K \cos(\lambda - \gamma_d + \beta) \cos \beta \sin \rho}{2 \sin \phi \cos(\phi - \gamma_d + \beta)} dl \quad (13)$$

The force element in the direction perpendicular to the cutting velocity and to the cutting edge

$$dF_T = dF_C \tan(\lambda - \gamma_d + \beta) \quad (14)$$

The force element in the direction perpendicular to  $dF_C$  and  $dF_T$

$$dF_F = \sqrt{(dF_C)^2 + (dF_T)^2} \sin \lambda \tan \eta \quad (15)$$

The total thrust force and torque are obtained by integrating the elemental cutting forces along the cutting edge.

$$F_L = 2 \int_{r_B}^{r_A} \sin \rho \, dF_T + 2 \int_{r_B}^{r_A} \cos \rho \, dF_F \quad (16)$$

$$T = 2 \int_{r_B}^{r_A} r \cos i \, dF_C + 2 \int_{r_B}^{r_A} r \sin i \sin \rho \, dF_F \quad (17)$$

## 2.2 The cutting forces prediction model and the method II

The method of Elhachimi is based on the principle of the calculation of the elements of the thrust and the torque for an element  $dl$  of the cutting edge at an arbitrary point on the cutting edge, situated at a radius  $r$  from the drill axis.

### 2.2.1 Geometrical model II and relationships

In this work, the authors identify two different regions of interest (the primary cutting edge and the chisel edge) and then estimate the thrust forces and torque for each region. The geometrical model is shown on Figure 2.3.

Dynamic rake angle

$$\gamma_n = \gamma_r - \varepsilon$$

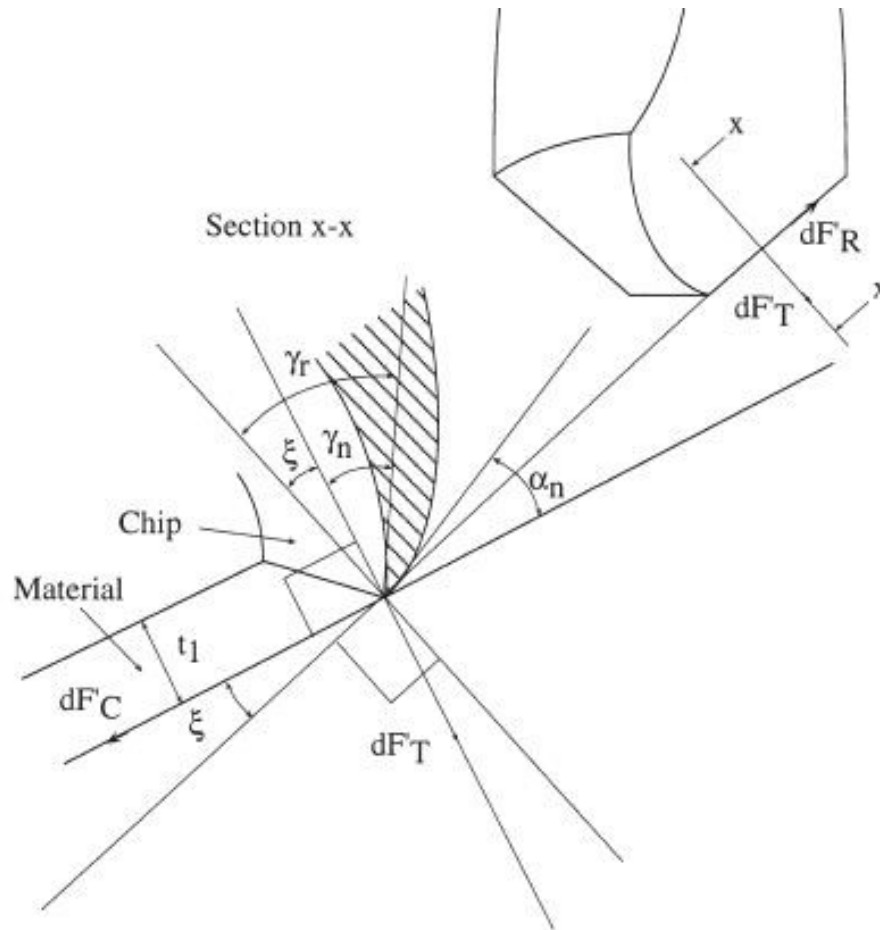


Figure 2.3. Dynamic geometry of the primary cutting edge by Elhachimi

where  $\varepsilon$  is the reference angle, which can be calculated as

$$\tan \varepsilon = \tan \omega \cos \rho \quad (19)$$

Static (normal) rake angle calculated by the formula

$$\tan \gamma_r = \frac{\tan \delta_r \cos \omega}{\sin \rho - \tan \delta_r \sin \omega \cos \rho} \quad (20)$$

whose credibility will be discussed later.

The differential element for the length of the cutting edge

$$dl = \frac{r}{\sin \rho \sqrt{(r^2 - t_p^2)}} dr \quad (21)$$

### 2.2.2. The force and torque prediction model II

The determination of the differential force and torque elements for each differential element of the cutting edge are also based on the above mentioned Oxley model [79]. Furthermore, the authors describe more precisely the way the elemental forces act at the arbitrary point of the cutting edge as shown on Figure 2.4.

The force element in the direction normal to the cutting edge in the plane constructed by the cutting edge and the cutting velocity vector

$$dF'_C = \frac{dF_S \cos(\phi - \gamma_d)}{\cos \theta} \quad (22)$$

The force in the direction normal to the machined surface

$$dF'_T = \frac{dF_S \sin(\phi - \gamma_d)}{\cos \theta} \quad (23)$$

And the force element in the direction perpendicular to  $F'_C$  and  $F'_T$

$$dF'_R = \left( \sqrt{dF'^2_C + dF'^2_T} \right) \sin \lambda \tan \eta \quad (24)$$

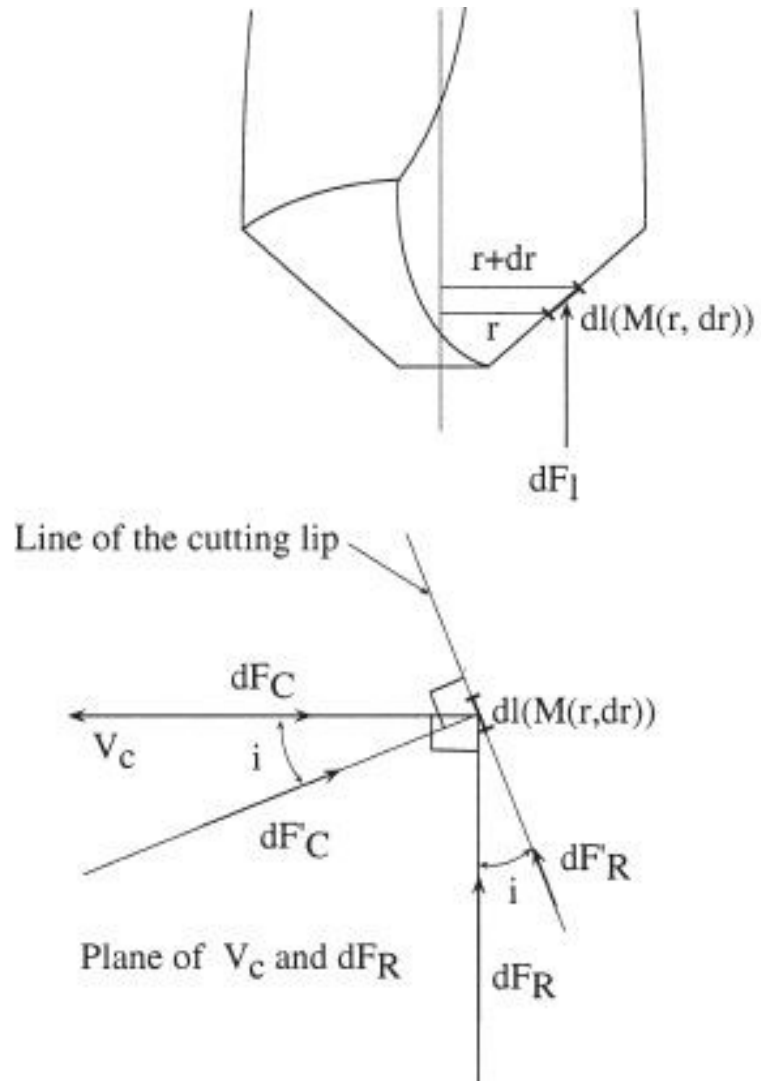


Figure 2.4. Force prediction model by Elhachimi.

where  $F_S$  is the shear force element [79] calculated as

$$F_S = \frac{Kfr \cos \varepsilon}{2 \sin \phi \sqrt{(r^2 - t^2)}} dr \quad (25)$$

Then, the force elements at the specific point are presented as

$$dF_C = dF'_C \cos i + dF'_R \sin i \quad (26)$$

$$dF_T = dF'_T \quad (27)$$

$$dF_R = dF'_R \cos i - dF'_C \sin i \quad (28)$$

The following formulas for the total thrust force and torque are:

$$F_L = \int_{r_B}^{r_A} \frac{fK_{TH} \sin \rho \cos \varepsilon}{\sin \phi \cos \theta} (\sin(\lambda - \gamma_d - \varepsilon) \sin \rho - \cos \rho) \frac{r}{\sqrt{(r^2 - t_p^2)}} dr \quad (29)$$

$$T = \int_{r_B}^{r_A} \frac{fK_{TQ} \sin \rho \cos \varepsilon}{\sin \phi \cos \theta} \cos(\phi - \gamma_d - i) \frac{r^2}{\sqrt{(r^2 - t_p^2)}} dr \quad (30)$$

### 2.3 The cutting forces prediction model and the method III

The method Armarego is also based on the principle of the calculation of the elements of the thrust and the torque for an element  $dl$  of the cutting edge at an arbitrary point on the cutting edge, situated at a radius  $r$  from the drill axis. The cutting

action is presented as a number of oblique cutting elements with its own geometry, cutting speed, feed, cut thickness and width of cut.

### 2.3.1 Geometrical model III and relationships

Probably the best description of the cutting edge geometry was given by Armarego [20] as it can be seen on Figure 2.5.

The normal rake angle  $\alpha_n$ , which is defined as an acute angle between the tangent to the cutting edge in the plane normal to the cutting edge and the normal to the projection of the cutting velocity in that plane.

$$\alpha_n = \alpha_{ref} - \varepsilon \quad (31)$$

And can be derived from the equations

$$\tan \alpha_{ref} = \frac{\tan \delta_r \cos \omega}{\sin \rho - \tan \delta_r \sin \omega \cos \rho} \quad (32)$$

and

$$\tan \varepsilon = \tan \omega \cos \rho \quad (33)$$

Combining these equations it is possible to define  $\alpha_n$

$$\tan \alpha_n = \frac{\tan \delta_r}{\sin \rho} (\cos \omega + \sin \omega \tan \omega \cos^2 \rho) - \tan \omega \cos \rho \quad (34)$$

### Geometrical derivation of rake angle

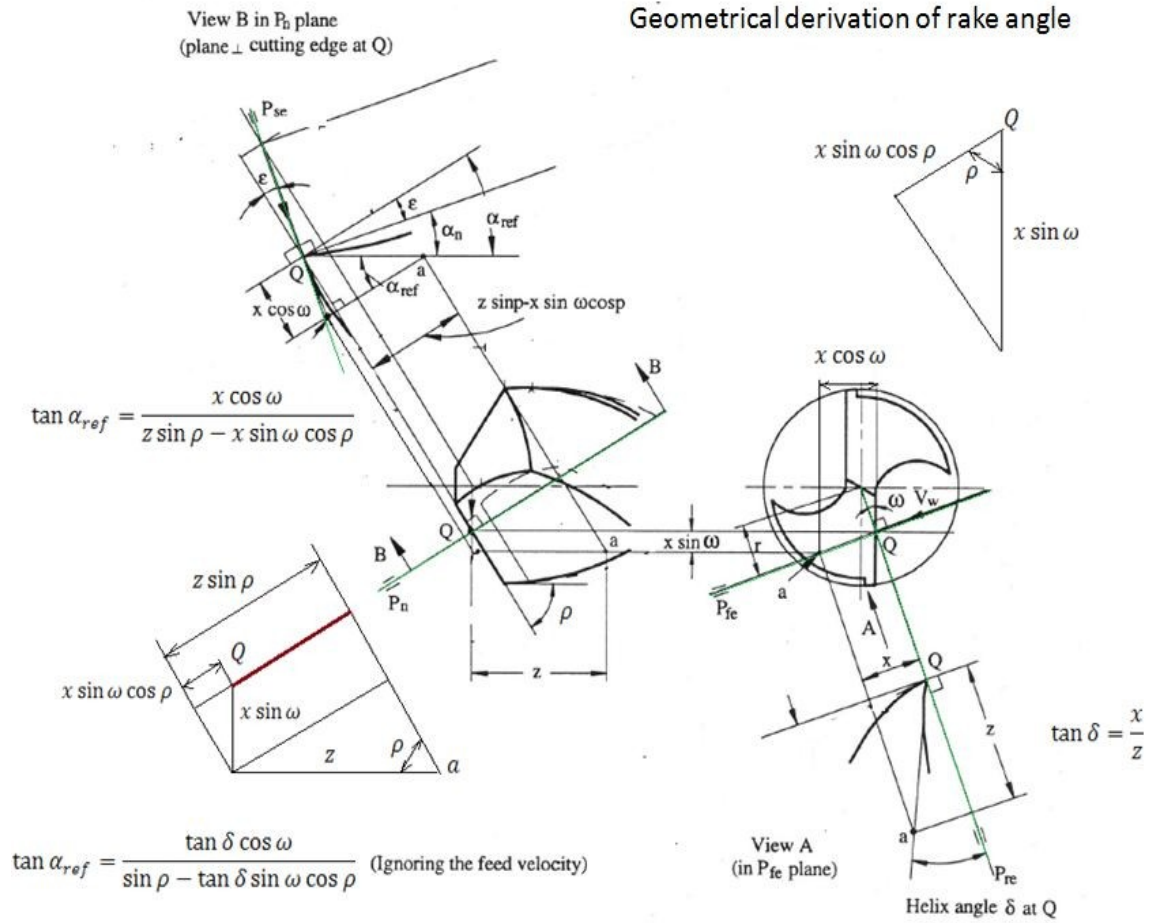


Figure 2.5. Dynamic geometry of the primary cutting edge by Armarego.

The normal friction angle in the plane normal to the cutting edge

$$\tan \beta_n = \tan \beta \cos \eta \quad (35)$$

The normal shear angle in the plane normal to the cutting edge

$$\tan \phi_n = \frac{r_c \frac{\cos \eta}{\cos i} \cos \alpha_n}{1 - r_c \cos \eta \cos i \sin \alpha_n} \quad (36)$$

where  $\beta$ ,  $\eta$  and  $r_c$  are the empirical friction angle, the empirical chip flow angle and the empirical chip thickness, respectively.

### 2.3.2. The force and torque prediction model III

Armarego believes that in the cutting action the forces may be divided by two main components: the “cutting” or deformation forces components due to the shearing and the friction processes on the shear plane and the rake face and the “edge” or classical oblique forces due to the ploughing or rubbing at the cutting edge as shown on Figure 2.6.

Then the elemental thrust force is

$$dF_L = (dF_Q + dF_{Qe}) \cos \varepsilon \sin \rho - (dF_R + dF_{Re})(\cos i \cos \rho + \sin i \sin \rho \sin \varepsilon) \quad (37)$$

and the elemental torque is

$$dT = r_i(dF_P + dF_{Pe}) \quad (38)$$

The total thrust force and torque are expressed as

$$F_L = 2 \sum_{i=1}^n dF_L \quad (39)$$

$$T = 2 \sum_{i=1}^n dT \quad (40)$$

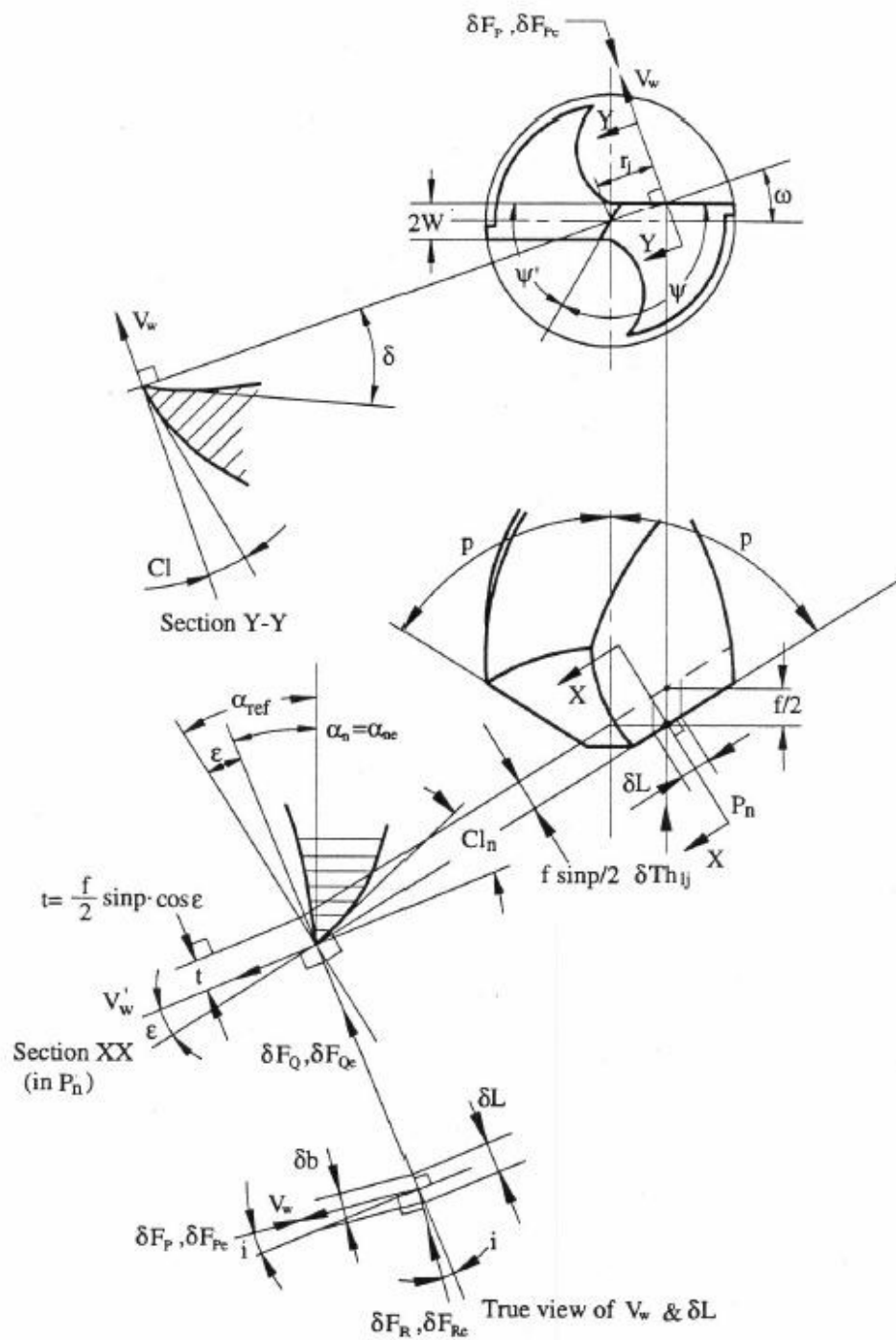


Figure 2.6. Force prediction model by Armarego

where  $dF_P$ ,  $dF_R$  and  $dF_Q$  are the cutting force components due to the shearing and the friction processes

$dF_{Pe}$ ,  $dF_{Re}$  and  $dF_{Qe}$  are the cutting forces due to the ploughing at the cutting edge

$n$  is the number of elements

$r_i$  is the mean radius of each element

$$dF_P = \frac{\tau dA (\cos(\beta_n - \alpha_n) \cos i + \tan \eta \sin i \sin \beta_n)}{B} \quad (41)$$

$$dF_R = \frac{\tau dA \sin(\beta_n - \alpha_n)}{B} \quad (42)$$

$$dF_Q = \frac{\tau dA (\cos(\beta_n - \alpha_n) \sin i - \tan \eta \cos i \cos \beta_n)}{B} \quad (43)$$

$$\text{where } B = \sin \phi \cos i \sqrt{\cos^2(\phi + \beta_n - \alpha_n) + \tan^2 \eta \sin^2 \beta_n} \quad (44)$$

$$dA = \frac{f \sin \rho \cos \varepsilon}{2} dl \cos i \quad (45)$$

$$dF_{Pe} = K_P dl \cos i \quad (46)$$

$$dF_{Qe} = K_Q dl \cos i \quad (47)$$

$$dF_{Re} = 0 \quad (48)$$

Empirical values  $K_P$ ,  $K_Q$  and  $\tau$  are taken from Armarego's cutting database.

## 2.4. Critical notes and discussion

There are a few mistakes in the geometrical analysis that were made by Chen.

The dynamic rake angle cannot be determined as

$$\gamma_d = \gamma_s + \beta$$

From Figure 2.5 it is clear that

$$\gamma_d = \gamma_s - \varepsilon$$

where  $\tan \gamma_s = \frac{x \cos \omega}{z \sin \rho - x \sin \omega \cos \rho}$  and since  $\tan \delta_r = \frac{x}{z}$

$$\tan \gamma_s = \frac{\tan \delta_r \cos \omega}{\sin \rho - \tan \delta_r \sin \omega \cos \rho}$$

The reference angle may be found from a geometrical analysis by projecting the tangential velocity in the normal plane.

From the same Figure 2.5  $\tan \varepsilon = \frac{V_W \sin \omega \cos \rho}{V_W \cos \omega} = \tan \omega \cos \rho$

Combining both equations

$$\gamma_d = \gamma_s - \varepsilon$$

$$\tan \gamma_d = \tan(\gamma_s - \varepsilon) = \frac{\tan \gamma_s - \tan \varepsilon}{1 + \tan \gamma_s \tan \varepsilon}$$

$$= \frac{\frac{\tan \delta_r \cos \omega}{\sin \rho - \tan \delta_r \sin \omega \cos \rho} - \tan \omega \cos \rho}{1 + \frac{\tan \delta_r \cos \omega \tan \omega \cos \rho}{\sin \rho - \tan \delta_r \sin \omega \cos \rho}}$$

$$= \frac{\frac{\tan \delta_r \cos \omega - \tan \omega \cos \rho (\sin \rho - \tan \delta_r \sin \omega \cos \rho)}{\sin \rho - \tan \delta_r \sin \omega \cos \rho}}{\frac{\sin \rho - \tan \delta_r \sin \omega \cos \rho + \tan \delta_r \cos \omega \tan \omega \cos \rho}{\sin \rho - \tan \delta_r \sin \omega \cos \rho}} =$$

$$= \frac{\tan \delta_r \cos \omega - \tan \omega \cos \rho (\sin \rho - \tan \delta_r \sin \omega \cos \rho)}{\sin \rho - \tan \delta_r \sin \omega \cos \rho + \tan \delta_r \cos \omega \tan \omega \cos \rho} =$$

$$= \frac{\tan \delta_r \cos \omega - \tan \omega \cos \rho (\sin \rho - \tan \delta_r \sin \omega \cos \rho)}{\sin \rho - \tan \delta_r \cos \rho (\sin \omega - \cos \omega \tan \omega)} =$$

$$= \frac{\tan \delta_r \cos \omega - \tan \omega \cos \rho \sin \rho + \tan \omega \tan \delta_r \sin \omega \cos^2 \rho}{\sin \rho}$$

and finally

$$\gamma_d = \frac{\tan \delta_r}{\sin \rho} (\cos \omega + \sin \omega \tan \omega \cos^2 \rho) - \tan \omega \cos \rho \quad (49)$$

which is different from the formula(6) presented by Chen

This formula can also be proved by using parametric derivation [78]

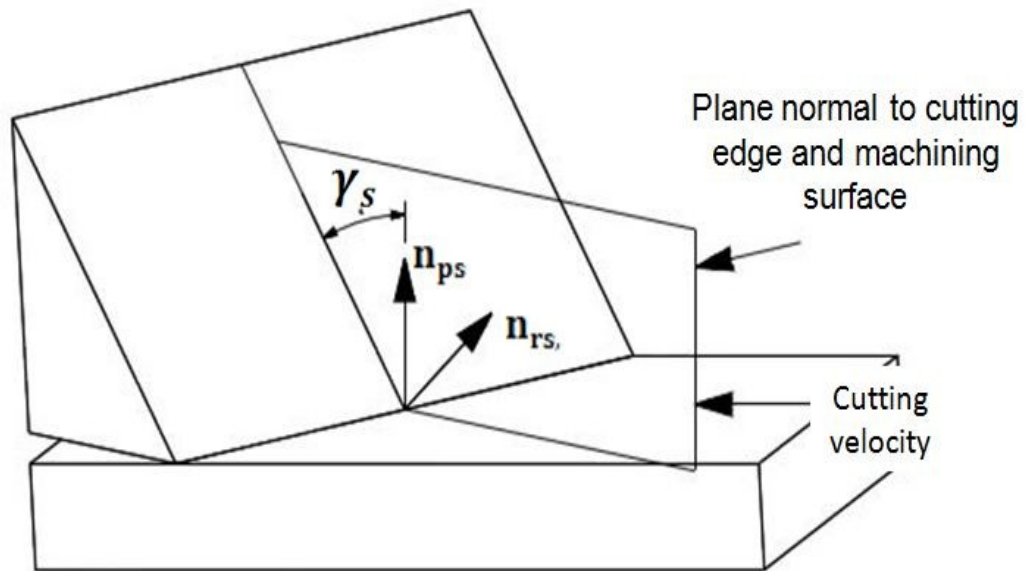


Figure 2.7. Parametrical model for the static rake angle derivation.

The static rake angle may be presented as

$$\gamma_s = 90 - \angle(\mathbf{n}_{rs}, \mathbf{n}_{ps}) \quad (50)$$

where

$\mathbf{n}_{ps}$  - unit normal vector to the tool cutting edge reference plane

$\mathbf{n}_{rs}$  - unit normal vector to the drill rake face

then

$$\mathbf{n}_{rs} \mathbf{n}_{ps} = |\mathbf{n}_{rs}| |\mathbf{n}_{ps}| \cos \angle(\mathbf{n}_{rs}, \mathbf{n}_{ps}) \quad (51)$$

$$|\mathbf{n}_{rs} \times \mathbf{n}_{ps}| = |\mathbf{n}_{rs}| |\mathbf{n}_{ps}| \sin \angle(\mathbf{n}_{rs}, \mathbf{n}_{ps}) \quad (52)$$

$$\frac{\mathbf{n}_{rs} \mathbf{n}_{ps}}{|\mathbf{n}_{rs} \times \mathbf{n}_{ps}|} = \cot \angle(\mathbf{n}_{rs}, \mathbf{n}_{ps}) = \tan(90 - \angle(\mathbf{n}_{rs}, \mathbf{n}_{ps})) = \tan \gamma_s$$

so

$$\frac{\mathbf{n}_{rs} \mathbf{n}_{ps}}{|\mathbf{n}_{rs} \times \mathbf{n}_{ps}|} = \tan \gamma_s \quad (53)$$

Unit normal vector to the tool cutting edge reference plane

$$\mathbf{n}_{ps} = \mathbf{c} \times \mathbf{v}_p \quad (54)$$

where

$\mathbf{c}$ -unit vector along the cutting edge

$$\mathbf{c} = -\vec{j} \sin \rho - \vec{k} \cos \rho \quad (55)$$

$\mathbf{v}_p$  -unit vector of the direction of primary motion within the tool cutting edge plane

$$\mathbf{v}_p = \vec{i} \cos \omega + \vec{j} \sin \omega \quad (56)$$

then,

$$\mathbf{n}_{ps} = \begin{bmatrix} i & j & k \\ 0 & -\sin \rho & -\cos \rho \\ \cos \omega & \sin \omega & 0 \end{bmatrix}$$

$$\mathbf{n}_{ps} = \begin{bmatrix} \cos \rho \sin \omega \\ -\cos \rho \cos \omega \\ \sin \rho \cos \omega \end{bmatrix} \quad (57)$$

The parametric equation for the helix

$$\vec{p} = \vec{i} a \cos \theta + \vec{j} a \sin \theta + \vec{k} b \theta \quad (58)$$

where  $a=r$ ,  $b = \frac{r}{\tan \delta_r} = r \cot \delta_r$ ,  $\theta = \omega$

$$\mathbf{p} = \begin{bmatrix} r \cos \omega \\ r \sin \omega \\ r \omega \cot \delta_r \end{bmatrix} \quad (59)$$

Tangent vector

$$\mathbf{p}'(\omega) = \frac{\partial \mathbf{p}}{\partial \omega} = \begin{bmatrix} -r \sin \omega \\ r \cos \omega \\ r \cot \delta_r \end{bmatrix} \quad (60)$$

Unit tangent vector that is tangent to the rake surface (tangent to the helix line of the rake surface)

$$\mathbf{t} = \frac{\mathbf{p}'(\omega)}{|\mathbf{p}'(\omega)|}$$

since

$$|\mathbf{p}'(\omega)| = \sqrt{(-r \sin \omega)^2 + (r \cos \omega)^2 + (r \cot \delta_r)^2} = r \sqrt{1 + (\cot \delta_r)^2}$$

$$|\mathbf{p}'(\omega)| = \frac{r}{\sin \delta_r} \quad (61)$$

so

$$\mathbf{t} = \begin{bmatrix} -\sin \delta_r \sin \omega \\ \sin \delta_r \cos \omega \\ \cos \delta_r \end{bmatrix} \quad (62)$$

Then it is possible to find  $\mathbf{n}_{rs}$

$$\mathbf{n}_{rs} = \mathbf{c} \times \mathbf{t} = \begin{bmatrix} i & j & k \\ 0 & \sin \rho & \cos \rho \\ -\sin \delta_r \sin \omega & \sin \delta_r \cos \omega & \cos \delta_r \end{bmatrix}$$

That leads to

$$\mathbf{n}_{rs} = \begin{bmatrix} \sin \rho \cos \delta_r - \cos \rho \cos \omega \sin \delta_r \\ -\cos \rho \sin \omega \sin \delta_r \\ \sin \rho \sin \omega \sin \delta_r \end{bmatrix} \quad (63)$$

Using formulas (57) and (63) it is possible to express the following as

$$\mathbf{n}_{rs} \mathbf{n}_{ps} =$$

$$(\sin \rho \cos \delta_r - \cos \rho \cos \omega \sin \delta_r)(\cos \rho \sin \omega) +$$

$$(-\cos \rho \sin \omega \sin \delta_r)(-\cos \rho \cos \omega) + (\sin \rho \sin \omega \sin \delta_r)(\sin \rho \cos \omega) =$$

$$\sin \rho \sin \omega (\cos \delta_r \cos \rho - \sin \rho \cos \omega \sin \delta_r)$$

and

$$\mathbf{n}_{rs} \times \mathbf{n}_{ps}$$

$$= \begin{bmatrix} i & j & k \\ \sin \rho \cos \delta_r - \cos \rho \cos \omega \sin \delta_r & -\cos \rho \sin \omega \sin \delta_r & \sin \rho \sin \omega \sin \delta_r \\ \cos \rho \sin \omega & -\cos \rho \cos \omega & \sin \rho \cos \omega \end{bmatrix}$$

$$= i \begin{bmatrix} -\cos \rho \sin \omega \sin \delta_r & \sin \rho \sin \omega \sin \delta_r \\ -\cos \rho \cos \omega & \sin \rho \cos \omega \end{bmatrix} -$$

$$j \begin{bmatrix} \sin \rho \cos \delta_r - \cos \rho \cos \omega \sin \delta_r & \sin \rho \sin \omega \sin \delta_r \\ \cos \rho \sin \omega & \sin \rho \cos \omega \end{bmatrix} +$$

$$\mathbf{k} \begin{bmatrix} \sin \rho \cos \delta_r - \cos \rho \cos \omega \sin \delta_r & -\cos \rho \sin \omega \sin \delta_r \\ \cos \rho \sin \omega & -\cos \rho \cos \omega \end{bmatrix} =$$

$$-\mathbf{j}(\sin^2 \rho \cos \delta_r \cos \omega - \cos \rho \sin \rho \sin \delta_r)$$

$$+ \mathbf{k}(\cos^2 \rho \sin \delta_r - \sin \rho \cos \rho \cos \omega \cos \delta_r)$$

Substituting and simplifying (53)  $\tan \gamma_s = \frac{n_{rs} n_{ps}}{|n_{rs} \times n_{ps}|}$

Leads to

$$\tan \gamma_s = \frac{\tan \delta_r}{\sin \rho} (\cos \omega + \sin \omega \tan \omega \cos^2 \rho) - \tan \omega \cos \rho$$

Chen in his geometrical model omits the reference angle and replaces it by the feed angle. However, the reference angle  $\varepsilon$  is very important, because it is the projection of the combined angle of the fundamental angles  $\omega$  and  $\rho$  in the plane normal to the cutting edge as it is shown in the Armarego model (Figure 2.5. and Figure 2.6.)

This misunderstanding also leads to the wrong determination of uncut chip thickness.

Chen determines it as

$$t_1 = \frac{f \sin \rho \cos \beta}{2}$$

## Section F-F

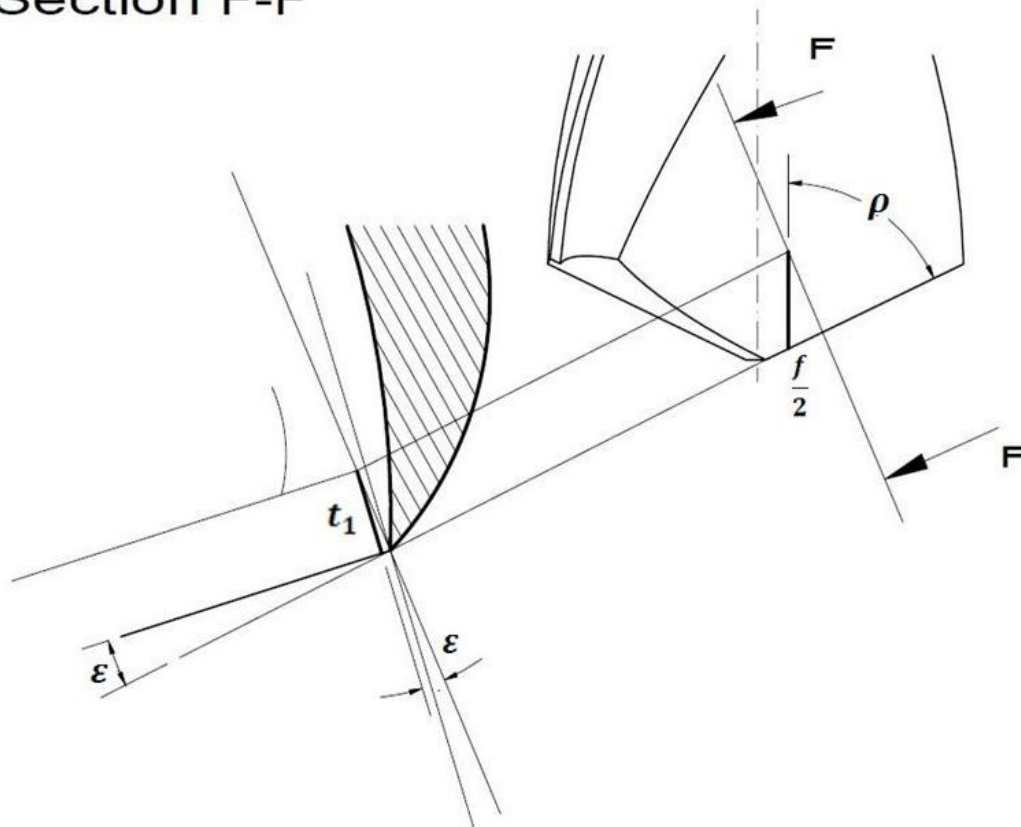


Figure 2.8. Uncut chip thickness

Clearly it must be defined as shown on Figure 2.8.

$$t_1 = \frac{f \sin \rho \cos \epsilon}{2} \quad (64)$$

Furthermore, the proposal of adding the feed angle to the force model seems to be questionable because in practice, the value of the resulting cutting speed is very close to the value of the tangential cutting speed and the axial feed component is negligible. The comparison between the dynamic and static rake angles for 8 mm drill (N=1000 rev/min and federate 0.12 mm) is shown on Figure 2.9.

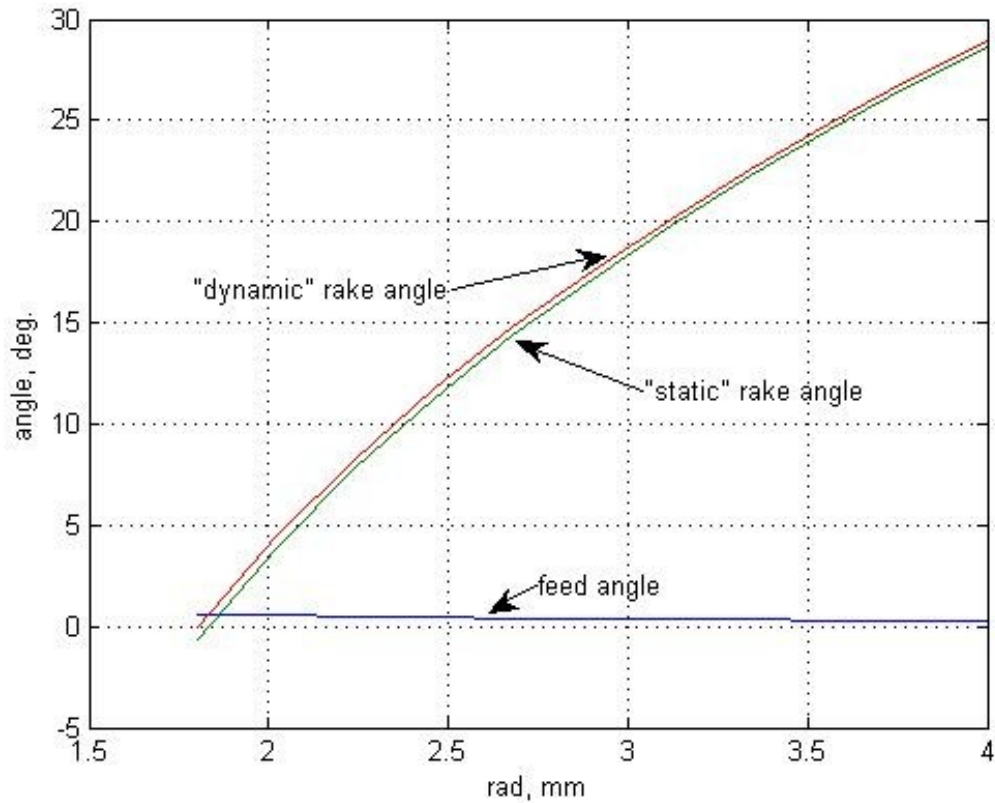


Figure 2.9. The distribution of the dynamic, static and feed angles along the cutting edge.

Thus, the adding of the feed angle  $\beta$  into the equations (13), (14) and (15)

doesn't properly reflect the actual projection of the elemental forces and also lacks the contribution of the inclination angle  $i$  in these equations.

The Elhachimi model describes the projection of the elemental forces more precisely.

The model contains a proper definition of the differential element of the cutting edge

$$dl = \frac{r}{\sin \rho \sqrt{(r^2 - t^2)}} dr \quad (65)$$

However, while Elhachimi tries to implement the Oxley force model, he makes a mathematical error in the formulas (29) and (30), when an incorrect substitution leads to a misleading result.

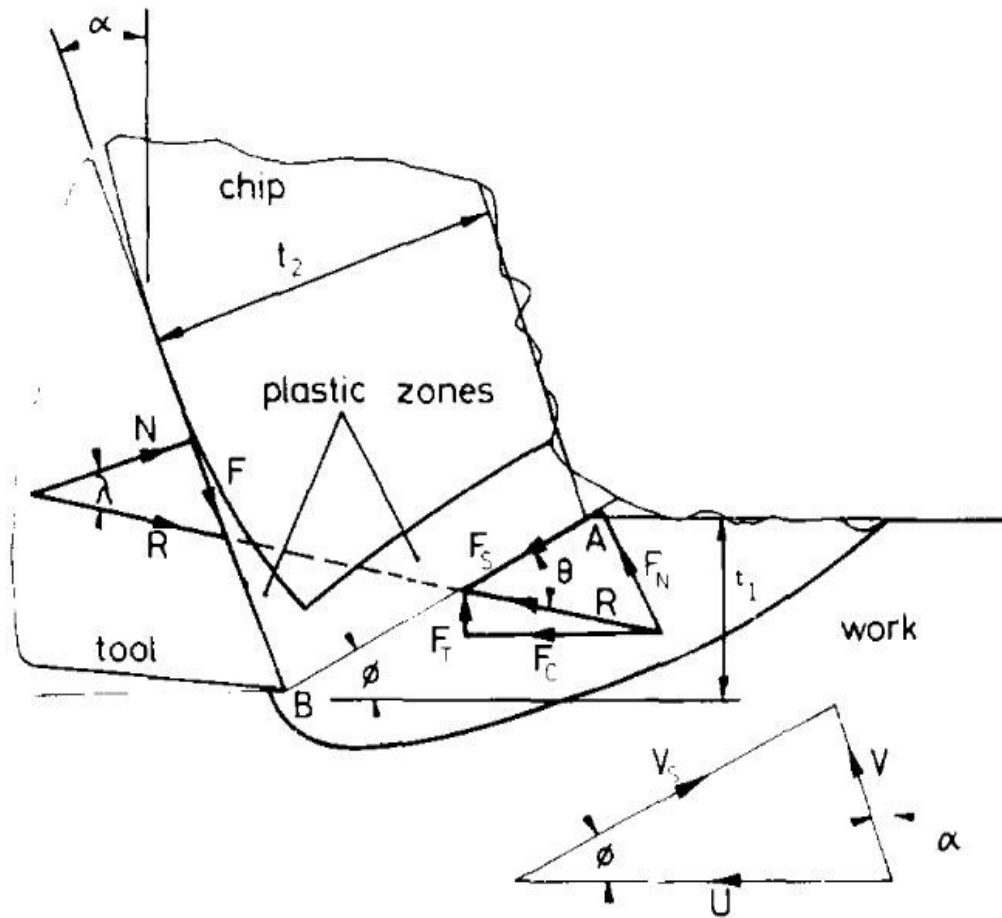


Figure 2.10. Oxley orthogonal chip formation model.

Following the Oxley model [79] the shear forces as shown on Figure 2.10. are

$$F_S = \frac{Kt_1dl}{\sin \phi} \quad (66)$$

$$R = \frac{F_S}{\cos \theta} \quad (67)$$

$$F_C = R \cos(\lambda - \gamma) \quad (68)$$

From there

$$F_C = \frac{F_S \cos(\lambda - \gamma)}{\cos \theta} \quad (69)$$

$$F_T = \frac{F_S \sin(\lambda - \gamma)}{\cos \theta} \quad (70)$$

$$\text{where } \theta = \phi - \gamma + \lambda \quad (71)$$

And this clearly contradicts with the formulas of Elhachimi

$$F_C = \frac{F_S \cos(\phi - \gamma)}{\cos \theta}$$

$$F_T = \frac{F_S \sin(\phi - \gamma)}{\cos \theta}$$

It leads to the wrong representation of  $F_R$  and then finally to the serious miscalculations in the proposed force model.

The Armarego model precisely describes the cutting edge geometry, but contains a lot of empirical formulas and requires the implementation of data from various orthogonal tests. The division of the cutting force into two components, the forces created by the

shearing and friction from one side and the forces created from the rubbing on other side is only assumed. It is extremely difficult to apply this approach since the "edge forces" have to be predetermined from each individual drilling test.

## Chapter 3. An improved method of cutting forces prediction

An improved method is based on the studying and analyzing of the three existing methods which were described in Chapter 2 and its purpose is to overcome the discovered drawbacks and errors. The new method presents the proper definitions of the dynamic rake angle and the uncut chip thickness, proves the negligibility of the feed angle and gives accurate representation of the elemental forces acting along the primary cutting edge, as well as the total thrust force and the torque. The cutting forces that are acting along the primary cutting edge are represented as a series of oblique cutting elements. The elemental forces are then integrated to determine the overall thrust force and drilling torque in terms of the basic geometrical features of the drill, the cutting conditions and the properties of the machined material.

### 3.1. Notations

$\phi_n$  shear angle of the orthogonal cutting

$\phi$  shear angle of the oblique cutting

$\theta$  angle of resulting force

$\lambda_n$	friction angle of the orthogonal cutting
$\lambda$	friction angle of the oblique cutting
$\gamma_s$	static rake angle
$\gamma_d$	dynamic rake angle
$\beta$	feed angle
$\delta_r$	helix angle at specified radius
$\delta$	helix angle at the diameter
$\omega$	web angle at specified radius
$\rho$	half-point angle
$i$	inclination angle
$t_p$	half web thickness before splitting point
$\varepsilon$	reference angle
$t_1$	uncut chip thickness
$K_{TH}$	shear stress factor induced by thrust forces
$K_{TQ}$	shear stress factor induced by torque
$K_{AB}$	shear stress factor
$\varepsilon_{AB}$	effective strain

$\dot{\epsilon}$	effective strain rate
$\gamma_{AB}$	shear strain
$\dot{\gamma}_{AB}$	shear strain rate
$V_S$	shear velocity
$dl$	differential element for the length of cutting edge
$dF_C$	elemental force parallel to the direction of the cutting velocity
$dF_T$	elemental force perpendicular to the direction of the cutting velocity and to the cutting edge (normal direction)
$dF_R$	elemental force perpendicular to the both $dF_C$ and $dF_T$ . (radial direction)
$\overline{dF_C}$	total elemental force in the direction of the cutting velocity
$\overline{dF_T}$	total elemental force in the normal direction
$\overline{dF_R}$	total elemental force in the radial direction
$dF_L$	total elemental thrust force
$dT$	total elemental torque

### 3.2 Derivation of improved formulas to predict total thrust and torque for the primary cutting edges

From the available Oxley force model [79] for oblique cutting, the elemental thrust force  $dF_L$  and the elemental torque can be determine based on the elemental forces  $dF_R$ ,  $dF_C$  and  $dF_T$  as can be seen on Figure 3.1.

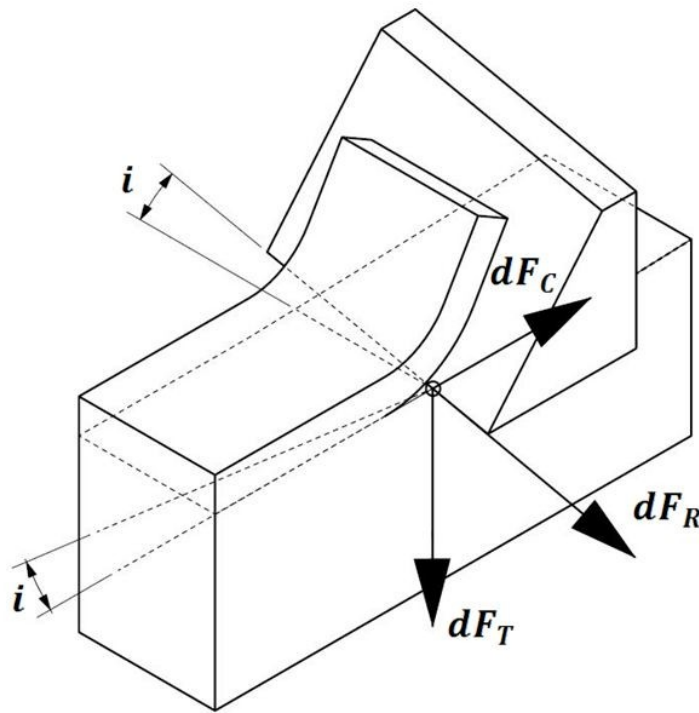


Figure 3.1. Oxley oblique cutting model.

The elemental force  $dF_C$  at any given point on the cutting edge is parallel to the direction of the cutting velocity, the elemental force  $dF_T$  is perpendicular to the direction of the cutting velocity and to the cutting edge and the elemental force  $dF_R$  is perpendicular to the both  $dF_C$  and  $dF_T$ .

The presented CAD model (Figure 3.2.) allows to derive the total thrust force accordingly the projections of each elemental force in each direction.

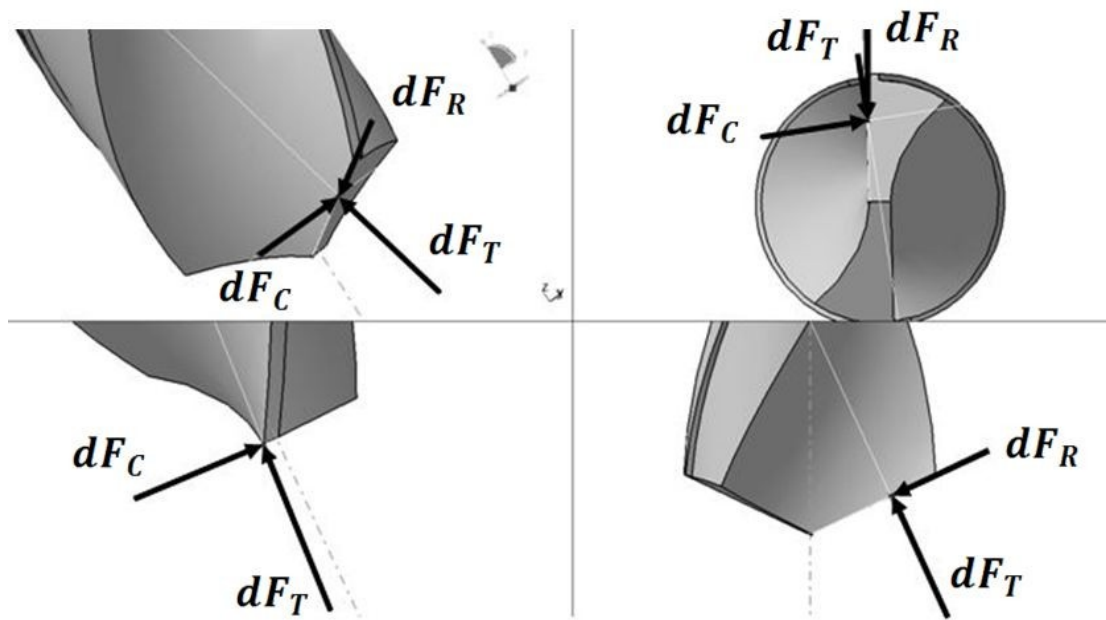


Figure 3.2. The projections of the elemental forces.

The total elemental forces  $\overline{dF_T}$ ,  $\overline{dF_R}$  and  $\overline{dF_C}$  in normal direction, radial direction and in the direction of the cutting velocity respectively can be calculated as (Figure 3.3.)

$$\overline{dF_T} = dF_T \cos \varepsilon - dF_C \sin \varepsilon \quad (72)$$

$$\overline{dF_R} = dF_R \cos i - dF_C \sin i \quad (73)$$

$$\overline{dF_C} = dF_C \cos i + dF_R \sin i \quad (74)$$

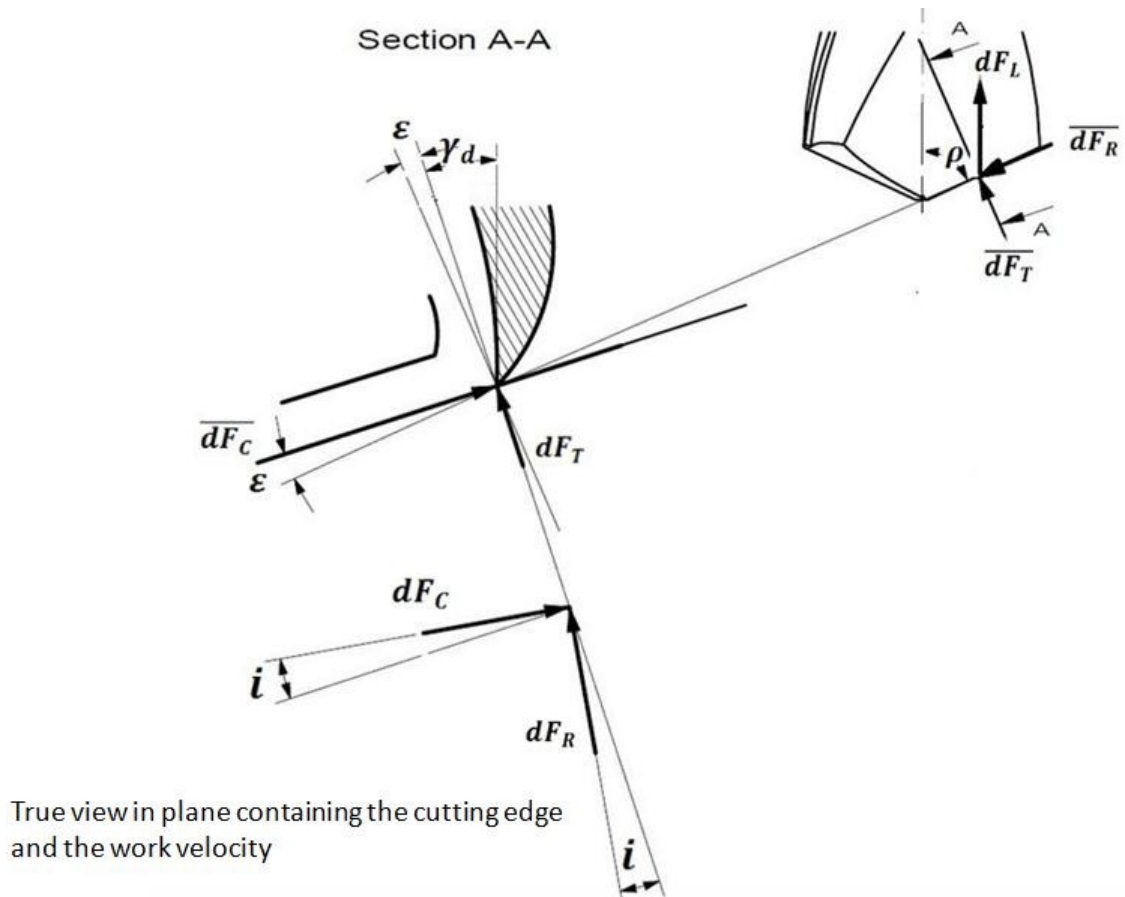


Figure 3.3. The model for force prediction along the primary cutting edge

Thereby

$$dF_L = \overline{dF_T} \sin \rho - \overline{dF_R} \cos \rho \quad (75)$$

So the total elemental thrust force can be expressed as

$$dF_L = (dF_T \cos \varepsilon - dF_C \sin \varepsilon) \sin \rho - (dF_R \cos i - dF_C \sin i) \cos \rho \quad (76)$$

or

$$dF_L = dF_T \cos \varepsilon \sin \rho - dF_C \sin \varepsilon \sin \rho - dF_R \cos i \cos \rho + dF_C \sin i \cos \rho \quad (77)$$

From the Oxley model [79]  $dF_T$  and  $dF_R$  can be found as

$$dF_R = \left( \sqrt{dF_C^2 + dF_T^2} \right) \sin \lambda \cos \gamma_d \tan i \quad (78)$$

$$dF_T = dF_C \tan(\lambda - \gamma_d) \quad (79)$$

substituting those formulas into (77)

$$dF_L =$$

$$dF_C \tan(\lambda - \gamma_d) \cos \varepsilon \sin \rho - \left( \sqrt{dF_C^2 + dF_T^2} \right) \sin \lambda \cos \gamma_d \tan i \cos i \cos \rho -$$

$$dF_C \sin i \cos \rho + dF_C \sin \varepsilon \sin \rho$$

And expressing this formula in terms of  $dF_C$

$$dF_L =$$

$$dF_C \tan(\lambda - \gamma_d) \cos \varepsilon \sin \rho -$$

$$\left( \sqrt{dF_C^2 + (dF_C \tan(\lambda - \gamma_d))^2} \right) \sin \lambda \cos \gamma_d \sin i \cos \rho - dF_C \sin i \cos \rho$$

$$+ dF_C \sin \varepsilon \sin \rho =$$

$$dF_C \tan(\lambda - \gamma_d) \cos \varepsilon \sin \rho - dF_C \left( \sqrt{1 + (\tan(\lambda - \gamma_d))^2} \right) \sin \lambda \cos \gamma_d \sin i \cos \rho -$$

$$dF_C \sin i \cos \rho + dF_C \sin \varepsilon \sin \rho$$

Then the total elemental thrust force can be calculated as

$$dF_L = dF_C \left( \tan(\lambda - \gamma_d) \cos \varepsilon \sin \rho - \frac{\sin \lambda \cos \gamma_d \sin i \cos \rho}{\cos(\lambda - \gamma_d)} - \sin i \cos \rho + \right. \\ \left. \sin \varepsilon \sin \rho \right) \quad (80)$$

From the orthogonal chip formation model using formulas (66), (67) and (68)

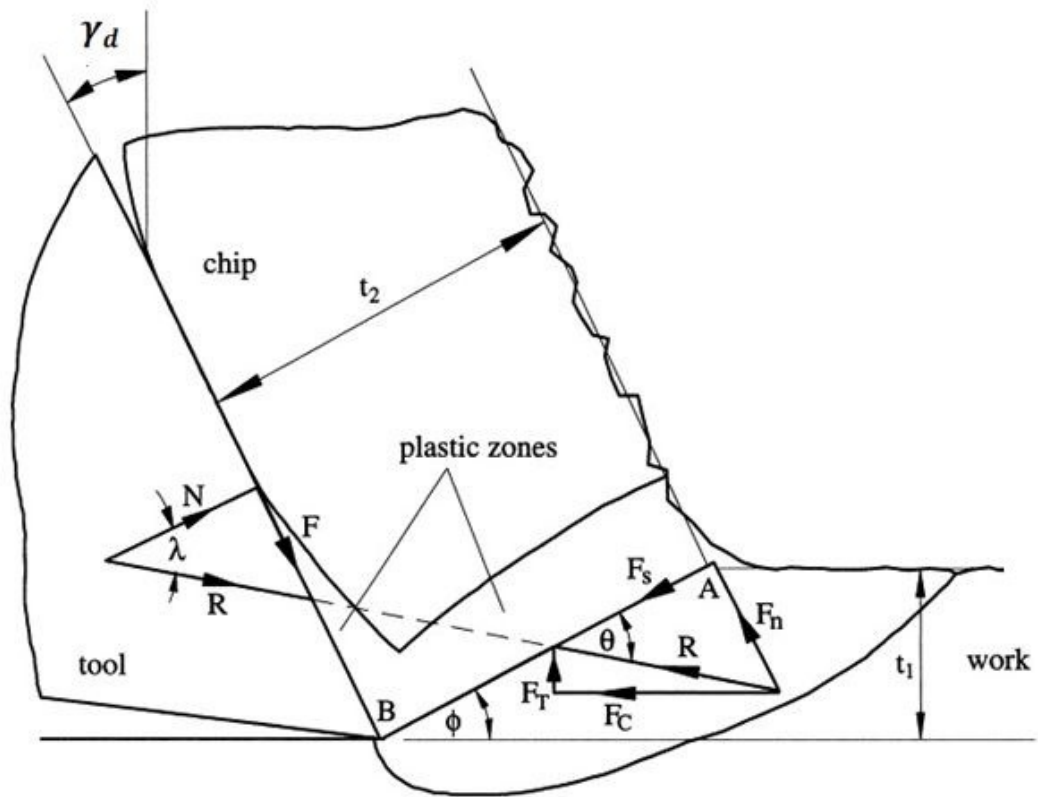


Figure 3.4. Orthogonal chip formation model for force prediction along the primary cutting edge

$$F_c = R \cos(\lambda - \gamma_d)$$

$$R = \frac{F_s}{\cos \theta}$$

$$F_s = \frac{K t_1 dl}{\sin \phi}$$

And the formula for the uncut chip thickness (64) from Figure 2.8

$$t_1 = \frac{f \sin \rho \cos \varepsilon}{2}$$

So the elemental force  $dF_C$  can expressed as

$$dF_C = \frac{f K_{AB} dl \cos(\lambda - \gamma_d) \cos \varepsilon \sin \rho}{2 \sin \phi \cos \theta} \quad (81)$$

where

$f$  feedrate

$K_{AB}$  shear stress factor

$dl$  differential element of the length of the cutting edge

Then

$$dF_L = \frac{f K_{AB} dl \cos(\lambda - \gamma_d) \cos \varepsilon \sin \rho}{2 \sin \phi \cos \theta} \left( \tan(\lambda - \gamma_d) \cos \varepsilon \sin \rho \right. \\ \left. - \frac{\sin \lambda \cos \gamma_d \sin i \cos \rho}{\cos(\lambda - \gamma_d)} - \sin i \cos \rho + \sin \varepsilon \sin \rho \right)$$

The differential element of the length of the cutting edge  $dl$  can be expressed as (21)

$$dl = \frac{r}{\sin \rho \sqrt{(r^2 - t_p^2)}} dr$$

Hence,

$$dF_L = \frac{f K_{AB} \cos(\lambda - \gamma_d) \cos \varepsilon \sin \rho}{2 \sin \phi \cos \theta} \left( \tan(\lambda - \gamma_d) \cos \varepsilon \sin \rho \right. \\ \left. - \frac{\sin \lambda \cos \gamma_d \sin i \cos \rho}{\cos(\lambda - \gamma_d)} \right. \\ \left. - \sin i \cos \rho + \sin \varepsilon \sin \rho \right) \frac{r}{\sin \rho \sqrt{(r^2 - t_p^2)}} dr$$

and finally

$$dF_L = \frac{f K_{AB} \cos(\lambda - \gamma_d) \cos \varepsilon}{2 \sin \phi \cos \theta} \left( \tan(\lambda - \gamma_d) \cos \varepsilon \sin \rho - \frac{\sin \lambda \cos \gamma_d \sin i \cos \rho}{\cos(\lambda - \gamma_d)} - \right. \\ \left. \sin i \cos \rho + \sin \varepsilon \sin \rho \right) \frac{r}{\sqrt{(r^2 - t_p^2)}} dr \quad (82)$$

From there it is possible to present the total thrust force

$$F_L = 2 \int_{r_B}^{r_A} dF_L$$

where  $[r_A, r_B]$  is an interval, which is defined by the radial distance from the drill axis to the beginning and the end of the primary cutting edge.

Therefore,

$$F_L = \int_{r_B}^{r_A} \frac{f K_{AB} \cos(\lambda - \gamma_d) \cos \varepsilon \sin \rho}{\sin \phi \cos \theta} \left( \tan(\lambda - \gamma_d) \cos \varepsilon \sin \rho - \frac{\sin \lambda \cos \gamma_d \sin i \cos \rho}{\cos(\lambda - \gamma_d)} - \sin i \cos \rho + \sin \varepsilon \sin \rho \right) \frac{r}{\sin \rho \sqrt{(r^2 - t_p^2)}} dr$$

or,

$$F_L = \int_{r_B}^{r_A} \frac{f K_{AB} \cos(\lambda - \gamma_d) \cos \varepsilon}{\sin \phi \cos \theta} \left( \tan(\lambda - \gamma_d) \cos \varepsilon \sin \rho - \frac{\sin \lambda \cos \gamma_d \sin i \cos \rho}{\cos(\lambda - \gamma_d)} - \sin i \cos \rho + \sin \varepsilon \sin \rho \right) \frac{r}{\sqrt{(r^2 - t_p^2)}} dr \quad (83)$$

The total elemental torque can be found as

$$dT = r \overline{dF_C} \quad (84)$$

where  $\overline{dF_C}$  is the total force in the direction of the cutting velocity, which can be calculated using the expression (74) (Figure 3.3.)

$$\overline{dF_C} = dF_C \cos i + dF_R \sin i$$

Implementing the same approach that was mentioned above the elemental torque can be expressed as

$$dT = r(dF_C \cos i + dF_R \sin i)$$

$$dT = r \left( dF_C \cos i + \left( \left( \sqrt{dF_C^2 + dF_T^2} \right) \sin \gamma_d \cos \gamma \tan i \right) \sin i \right) \quad (85)$$

From the Oxley model  $dF_T$  and  $dF_R$  can be expressed as

$$dF_R = \left( \sqrt{dF_C^2 + dF_T^2} \right) \sin \lambda \cos \gamma_d \tan i \quad (86)$$

$$dF_T = dF_C \tan(\lambda - \gamma_d) \quad (87)$$

substituting those formulas into (85) and expressing this formula in terms of  $dF_C$

$$\begin{aligned} dT &= r \left( dF_C \cos i + \left( \left( \sqrt{dF_C^2 + (dF_C \tan(\lambda - \gamma_d))^2} \right) \sin \lambda \cos \gamma_d \tan i \right) \sin i \right) = \\ &= r \left( dF_C \cos i + \left( \frac{dF_C}{\cos(\lambda - \gamma_d)} \sin \lambda \cos \gamma_d \tan i \right) \sin i \right) = \\ &= r dF_C \left( \cos i + \frac{\sin \lambda \cos \gamma_d \tan i \sin i}{\cos(\lambda - \gamma_d)} \right) \end{aligned}$$

Since the elemental force  $dF_C$  is presented in (81)

$$dF_C = \frac{f K_{AB} dl \cos(\lambda - \gamma_d) \cos \varepsilon \sin \rho}{2 \sin \phi \cos \theta}$$

and the differential element of the length of the cutting edge  $dl$  can be presented in (21)

$$dl = \frac{r}{\sin \rho \sqrt{(r^2 - t_p^2)}} dr$$

Hence,

$$dT = \frac{fr K_{AB} dl \cos(\lambda - \gamma_d) \cos \varepsilon \sin \rho \left( \cos i + \frac{\sin \lambda \cos \gamma_d \tan i \sin i}{\cos(\lambda - \gamma_d)} \right)}{2 \sin \phi \cos \theta} =$$

$$= \frac{f K_{AB} \cos(\lambda - \gamma_d) \cos \varepsilon}{2 \sin \phi \cos \theta} \frac{r^2}{\sqrt{(r^2 - t_p^2)}} \left( \cos i + \frac{\sin \lambda \cos \gamma_d \tan i \sin i}{\cos(\lambda - \gamma_d)} \right) dr$$

and finally

$$dT = \frac{f K_{AB} \cos \varepsilon}{2 \sin \phi \cos \theta} \frac{r^2}{\sqrt{(r^2 - t_p^2)}} \left( \frac{\cos i}{\cos(\lambda - \gamma_d)} + \sin \lambda \cos \gamma_d \tan i \sin i \right) dr \quad (88)$$

From there it is possible to present the total torque as

$$T = 2 \int_{r_B}^{r_A} dT \quad (89)$$

or

$$T = \int_{r_B}^{r_A} \frac{f K_{AB} \cos \varepsilon}{\sin \phi \cos \theta} \left( \frac{\cos i}{\cos(\lambda - \gamma_d)} + \sin \lambda \cos \gamma_d \tan i \sin i \right) \frac{r^2}{\sqrt{(r^2 - t_p^2)}} dr \quad (90)$$

All the parameters in both equations for the total thrust force and torque depend only on the radius of a point of the cutting edge from the drill axis and on the drill geometry and can be found from the equations (4),(5),(49),(8),(3),(12),(1),(2),(71) and (19).

$$i = \sin^{-1}(\sin \omega \sin \rho)$$

$$\omega = \sin^{-1} \frac{t_p}{r}$$

$$\gamma_d = \tan^{-1} \left( \frac{\tan \delta_r}{\sin \rho} (\cos \omega + \sin \omega \tan \omega \cos^2 \rho) - \tan \omega \cos \rho \right)$$

$$\delta_r = \tan^{-1} \left( \frac{2r}{D} \tan \delta \right)$$

$$\lambda = \tan^{-1} \left( \frac{\cos \phi - \cos \phi_n + \tan(\lambda_n - \gamma_d) \sin \phi_n}{\sin \phi} \right) + \gamma_d$$

$$\lambda_n = \frac{\pi}{6} + \frac{\gamma_d}{2}$$

$$\phi = \cot^{-1}(\cot \phi_n \cos i - \tan \gamma_d (1 - \cos i))$$

$$\phi_n = \frac{\pi}{4} + \frac{\gamma_d - \lambda_n}{2}$$

$$\theta = \phi + \lambda - \gamma_d$$

$$\varepsilon = \tan^{-1}(\tan \omega \cos \rho)$$

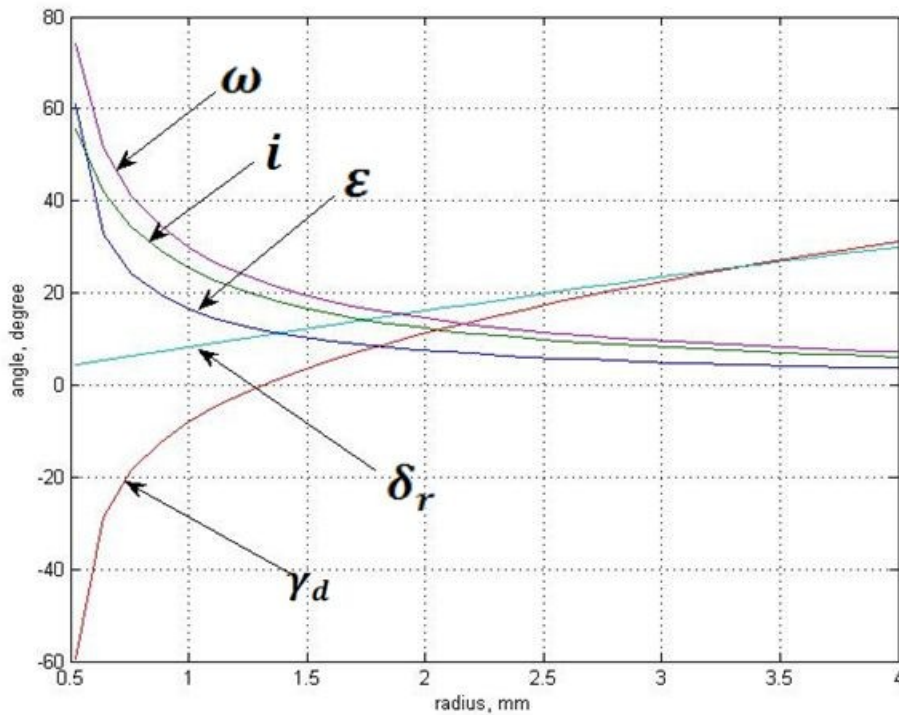


Figure 3.5. Distribution of the various angles along the primary cutting edge on 8 mm standard twist drill.

The distribution of the various angles along the primary cutting edge on 8 mm standard twist drill is shown on Figure 3.5.

The next important step in this calculation is the necessity to determine the shear stress factor  $K_{AB}$ , which essentially affects the values of the total thrust force and the torque.

Elhachimi completely omits this issue in his work [34], Chen applies the empirical formulas [36] based on the Oxley model and Armarego [20] uses his own empirical databank.

The Oxley algorithm [79] for the calculation of the shear stress factor can be used though it contains assumptions and repetitive interpolations. For example, for the given cutting conditions and material properties of carbon steel JIS S 45C (the same as AISI 1045), the below described procedure has to be applied.

The given formula for the shear stress factor

$$K_{AB} = \frac{\sigma_1 \varepsilon_{AB}^n}{\sqrt{3}} \quad (91)$$

where

$$\varepsilon_{AB} = \frac{\gamma_{AB}}{\sqrt{3}} \quad (92)$$

$$\gamma_{AB} = \frac{1}{2} \frac{\cos \gamma}{\sin \phi \cos(\phi - \gamma)} \quad (93)$$

The first step is to assume the given temperature  $T$  and then to estimate the flow stress  $\sigma_1$ , using the empirical formula or the presented diagram.

The next step is to determine the strain-hardening index  $n$ , which is a function of the temperature. It is then necessary to calculate  $\gamma_{AB}$ ,  $\varepsilon_{AB}$  and  $K_{AB}$  again using either the empirical formula or the diagram.

Since the actual temperature, the so called velocity modified temperature is yet unknown it has to be found by applying the following formula

$$T_{mod} = T \left( 1 - v \log \frac{\dot{\varepsilon}}{\dot{\varepsilon}_0} \right) \quad (94)$$

where

$$v = 0.09$$

$$\dot{\epsilon}_0 = 1, s^{-1}$$

$$\dot{\epsilon} = \dot{\epsilon}_{AB} = \frac{\dot{\gamma}_{AB}}{\sqrt{3}}$$

$$T = T_{AB} + 273^\circ C$$

Then the old and the new values of the velocity modified temperature should be compared and if the difference is significant the interpolation process must be continued until a reasonable difference is achieved.

The main problem in the Oxley algorithm is to find  $T_{AB}$  because  $F_S$  is indeterminate which leads to multiply interpolations until a desirable result is obtained.

Shear strain rate at AB by Oxley

$$\dot{\gamma}_{AB} = C \frac{V_S}{l} \quad (95)$$

$C$  is constant,  $C=5.9$

Shear velocity  $V_S$

$$V_S = \frac{v \cos \gamma}{\cos(\phi - \gamma)} \quad (96)$$

Length AB (from the orthogonal chip formation model)

$$l = \frac{t_1}{\sin \phi}$$

And since,

$$t_1 = \frac{f \sin \rho \cos \epsilon}{2}$$

Shear strain rate

$$\dot{\gamma}_{AB} = C \frac{2V \cos \gamma \sin \phi}{f \cos(\phi - \gamma) \sin \rho \cos \varepsilon} \quad (97)$$

which is different from Chen's formula

$$\dot{\gamma}_{AB} = \frac{2V \cos \gamma \sin \phi}{f \cos(\phi - \gamma)} \quad (98)$$

Chen [36] suggests that it is reasonable to assume that the shear stress factor is the function of the mean shear-strain rate  $\dot{\gamma}_{AB}$  in the corresponding region of the cutting edge and offers the following formulas which were obtained by a regression analysis for specific materials (particularly for 1015 steel).

Shear stress factor for the primary cutting edge induced by trust force

$$K_{TH} = 12.77 \log \dot{\gamma}_{AB} - 24.38 \quad (99)$$

Shear stress factor for the primary cutting edge induced by torque

$$K_{TQ} = 2.72 \log \dot{\gamma}_{AB} - 8.65 \quad (100)$$

Where  $\dot{\gamma}_{AB}$  is calculated by (98)

Both approaches for the determination of the shear stress factor can be applied, however for comparison purposes the formulas (99) and (100) were used.

## Chapter 4. Applications

The calculated values of the shear stress factor for any specific material (steel ANSI 1015 was used for the comparison analysis) allowed to find the predicted total thrust force and the total torque.

The comparison was made for the 8.00 mm HSS standard 118 degree twist drill on the ANSI 1020 steel with constant 1000 rpm and a feedrate of 0.12 mm/rev

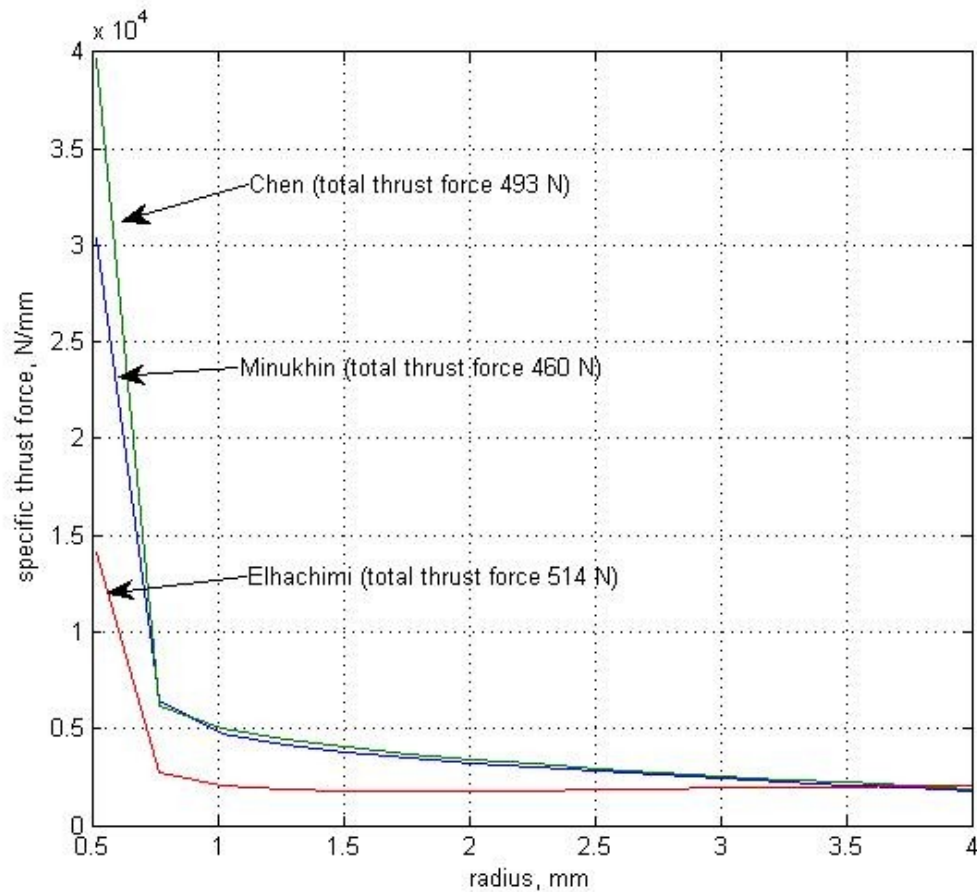


Figure 4.1. Comparison of predicted thrust forces for 8 mm standard twist drill.

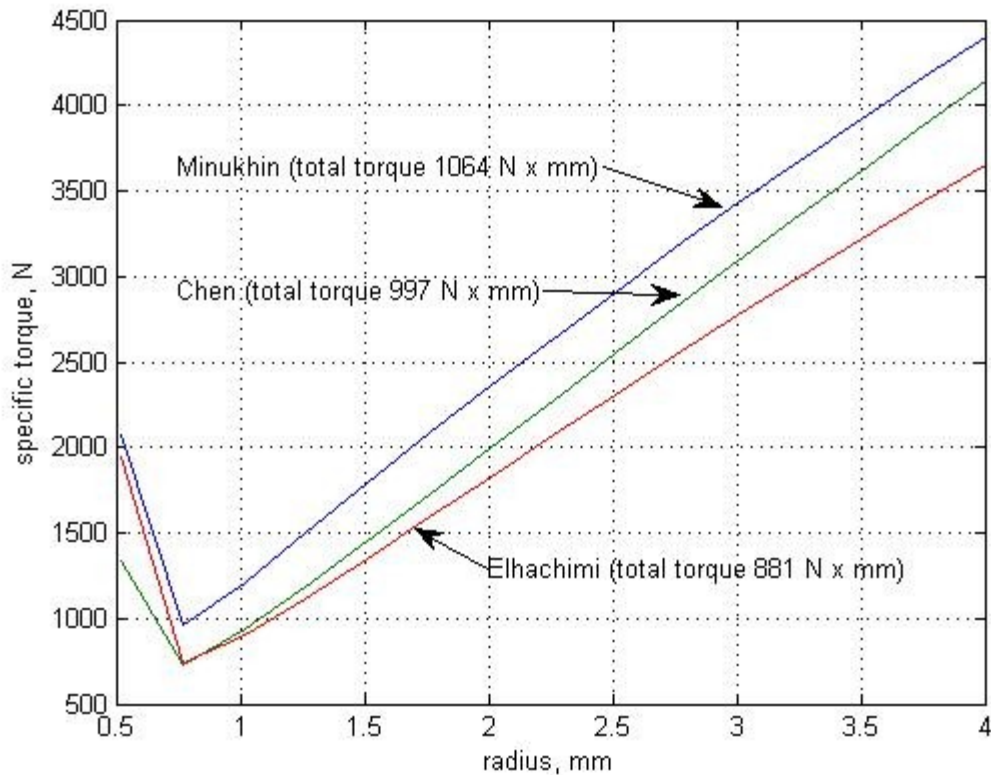


Figure 4.2. Comparison of predicted torques for 8 mm standard twist drill.

The total thrust force and torque expressed in formulas (16), (17), (29), (30), (83) and (90) in each method respectively were calculated using Matlab, the following graphical representations which show the distribution of the total thrust and torque along the primary cutting edge as well as the total values were generated, as can be seen on Figure 4.1. and Figure 4.2.

The ThirdWave FEM software simulation for the 8.00 mm HSS standard 118 degree twist drill on the ANSI 1020 steel with constant 1000 rpm and a feedrate of 0.12 mm/rev shows the following average values:

Total thrust force = 1256 N

Torque = 3321N mm

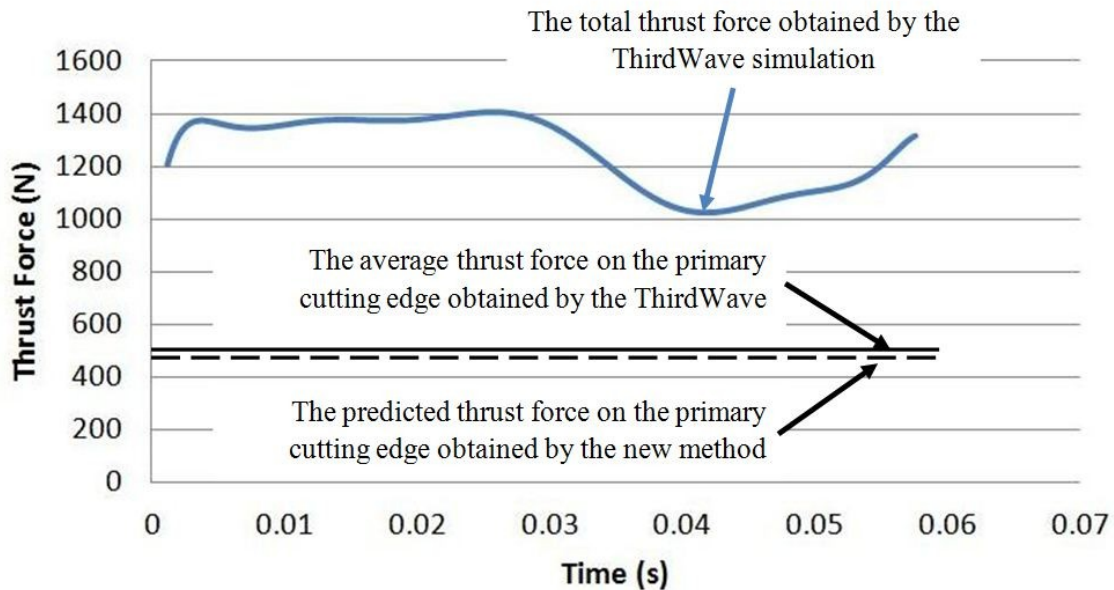


Figure 4.3. Prediction of thrust forces using ThirdWave simulation.

The calculations made with the original formulas(83) and (90) for the primary cutting edge show the following values for the total thrust force and torque respectively

$$F_L = 460 N$$

$$T = 989 N mm$$

Considering the empirical observations (Figure 4.4.) that the percentage of the total thrust forces and torque acting on the primary cutting edges for the conventional twist drill is approximately 40% and 80% respectively [72], the predicted values will be:

$$F_L(\text{by FEM}) = 1256 \times 40\% = 502 N$$

$$T(\text{by FEM}) = 3321 \times 80\% = 2657 \text{ N mm}$$

And it shows a fair agreement with the predicted data. The discrepancies may be explained by the uncertainty in the calculation of the shear stress factor.

The percentage of the total thrust forces and torque acting on the primary cutting edge, the chisel edge, and the margin for two different types of drills

Drill types	Cutting forces	Primary cutting edge	Chisel edge	Margin
Conventional twist drill	Thrust force	40	57	3
	Torque	80	8	12
Thick web drills	Thrust force	30	70	–
	Torque	68	20	12

Figure 4.4. Percentage of the total thrust forces and torques acting on the primary cutting edge and chisel edges for different types of twist drills.

Unfortunately, there is not enough experimental data for a comparison analysis to be found. J. S. Strenkowski, et al. [49], while developing an analytical finite element technique for predicting the thrust force and torque have provided experimental data, which was used for other comparisons. The drilling tests were performed on a Bridgeport using a high speed steel twist drill with a 30 degree helix angle and a 118 degree point angle. The workpiece was an AISI 1020 steel block. A spindle speed of 302 rpm was used. Three drills with 6.35, 9.53, and 12.5 mm diameters were used for three feed rates of 0.051, 0.076, and 0.102 mm/rev.

The calculations show a satisfying agreement between the measured and the predicted values, as seen on Figure 4.5.

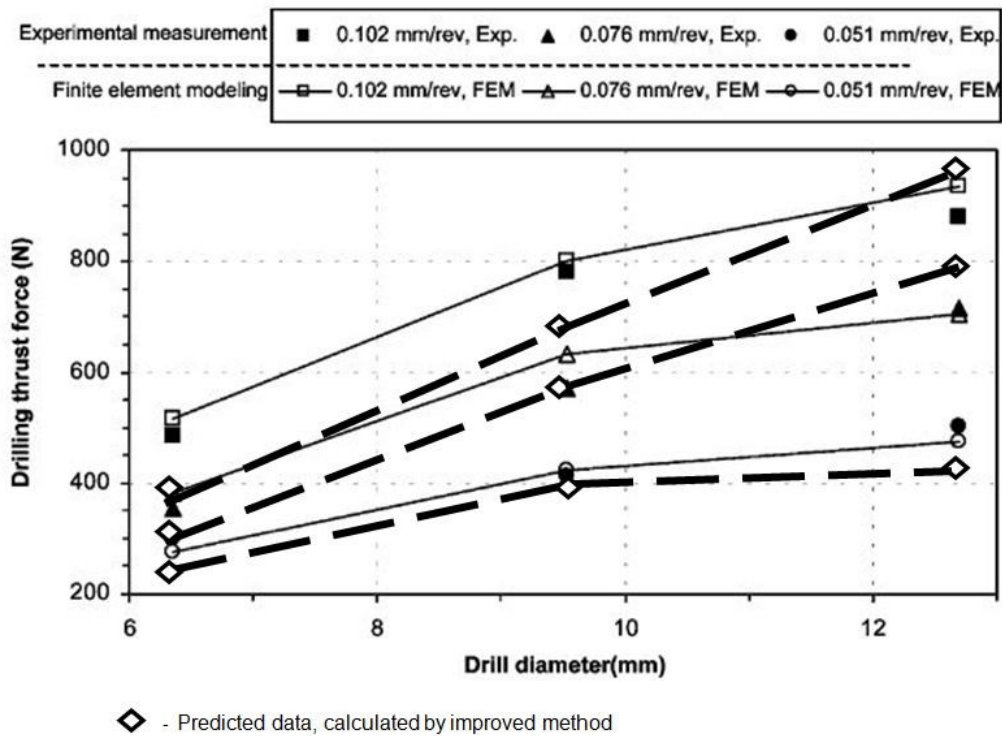
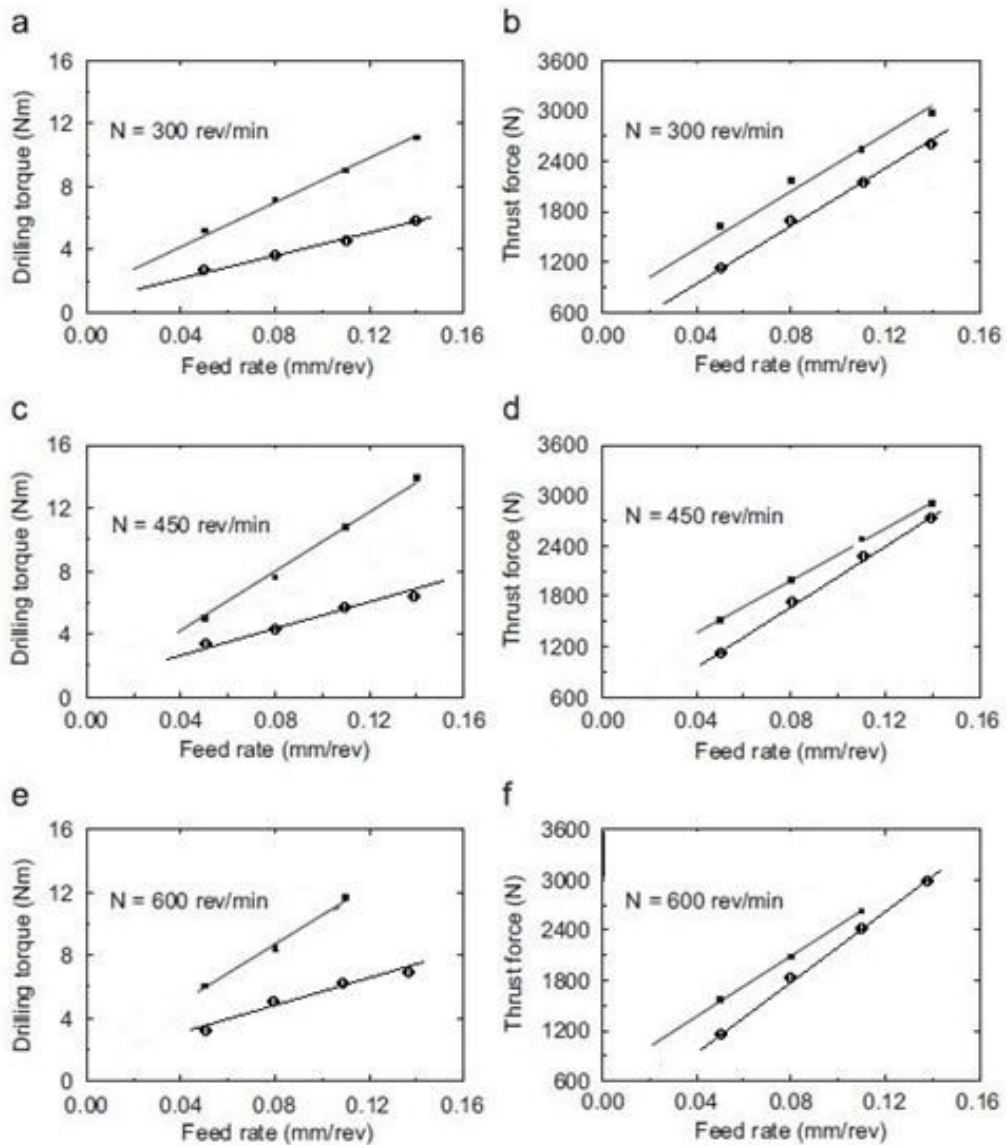


Figure 4.5. Comparison of predicted and experimental thrust forces based on test of Strenkowski

Another comparison was made based on the data provided by Xiong [77], who completed tests on the 1050 carbon steel, using conventional, straight-edged, HSS 15 mm diameter twist drill with the following dimensions: helix angle  $60^\circ$ , point angle  $118^\circ$ , web thickness 2.25 mm. The results are shown on Figure 4.6.

As previously mentioned, it is difficult to determine the values for the shear stress factor, but considering the fact that the hardness of the 1050 steel is 197 HB and the hardness of the 1025 steel is 126 HB [81] it is possible to assume that the predicted data will interpolate accordingly.



● Predicted data by improved method

Figure 4.6. Comparison of predicted and experimental thrust forces and torques, based on test of Xiong.

The improved method also allows to predict the thrust force and torque for the drills with various diameters, as seen on Figure 4.7. and Figure 4.8.

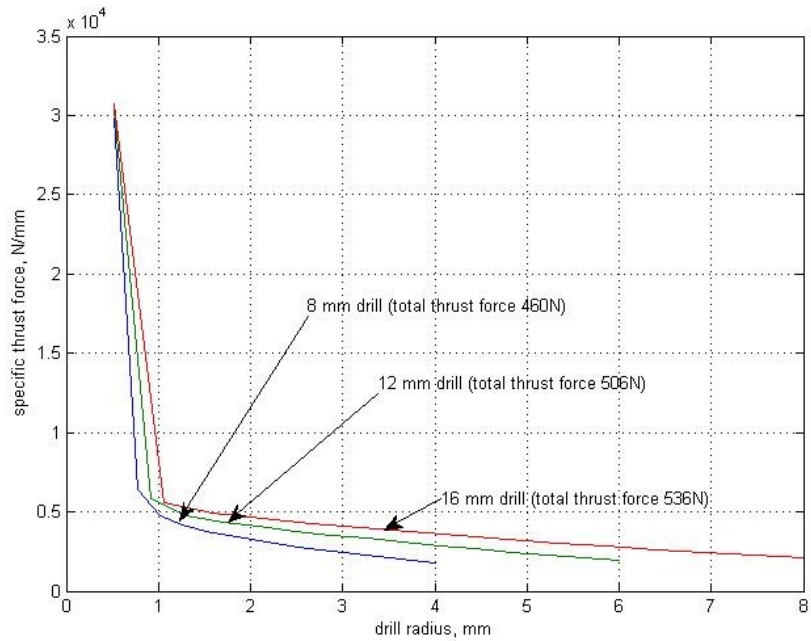


Figure 4.7. Predicted thrust forces for the standard 8, 12 and 16 mm twist drills

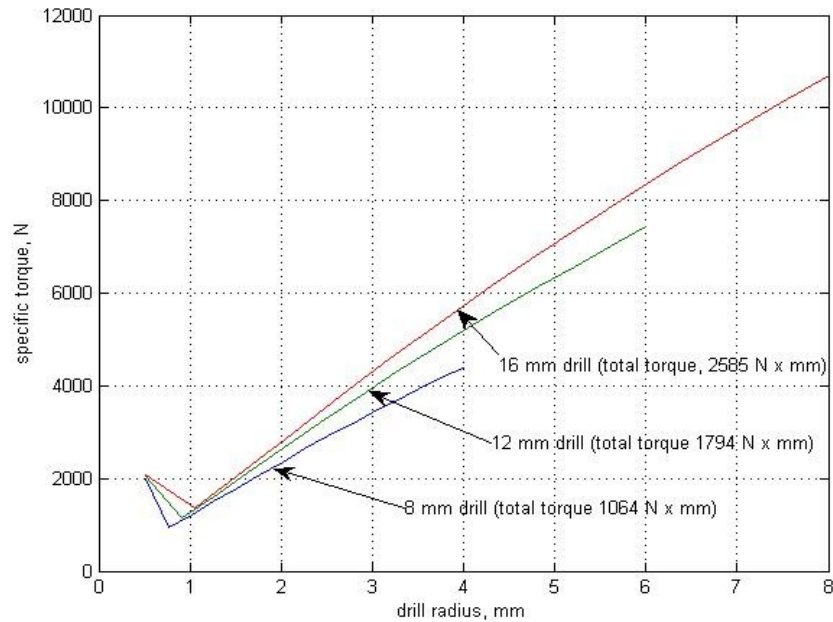


Figure 4.8. Predicted torques for the standard 8, 12 and 16 mm twist drills.

The formulas (83) and (90) show that the thrust force and torque can be calculated using the basic drill geometry features, such as the point angle  $\rho$ , the helix angle  $\delta$  and the half-web thickness  $t_p$ . It is therefore possible to determine how each feature affects the thrust forces and torque.

An increase of the point angle  $\rho$  leads to the decrease of the thrust force and the increase of the torque as seen on Figure 4.9. and Figure 4.10.

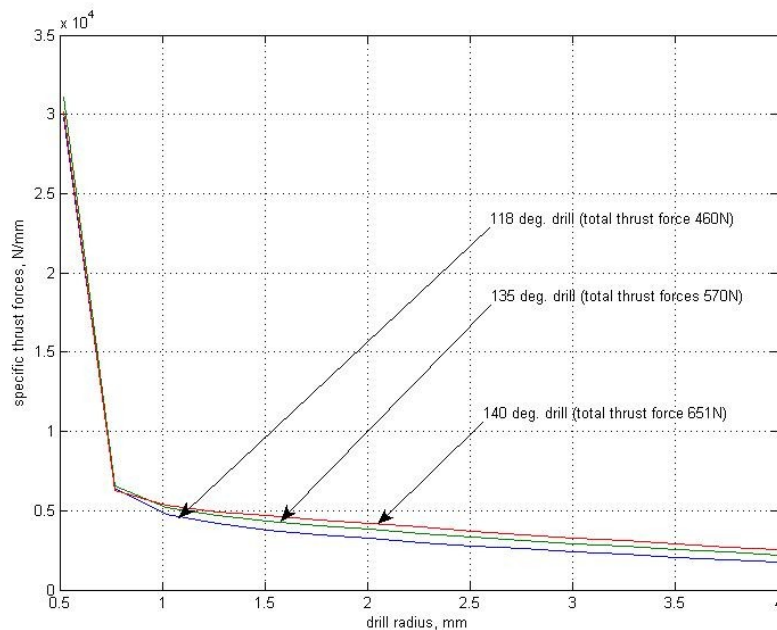


Figure 4.9. Predicted thrust forces for the standard 8mm twist drill with the 118°, 135° and 140° point angles

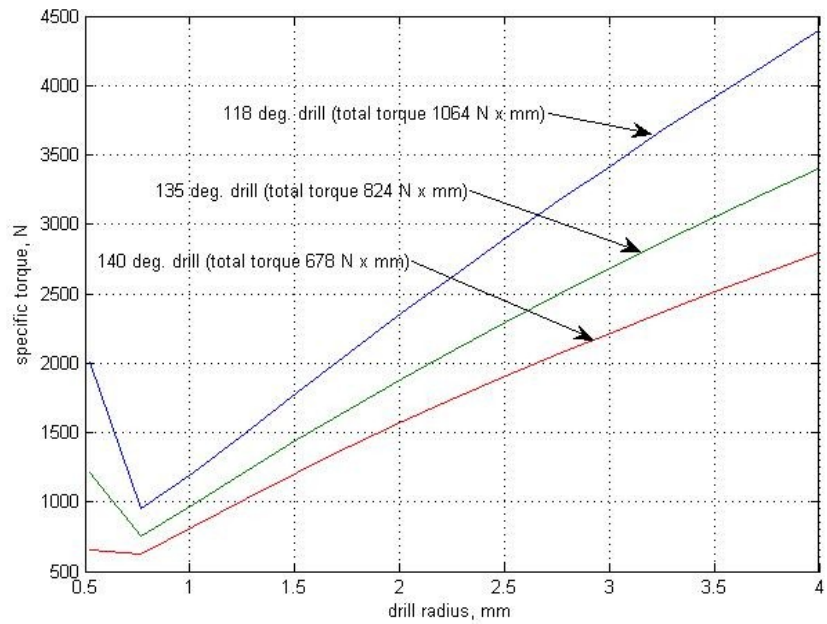


Figure 4.10. Predicted torques for the standard 8mm twist drill with the 118°, 135° and 140° point angles

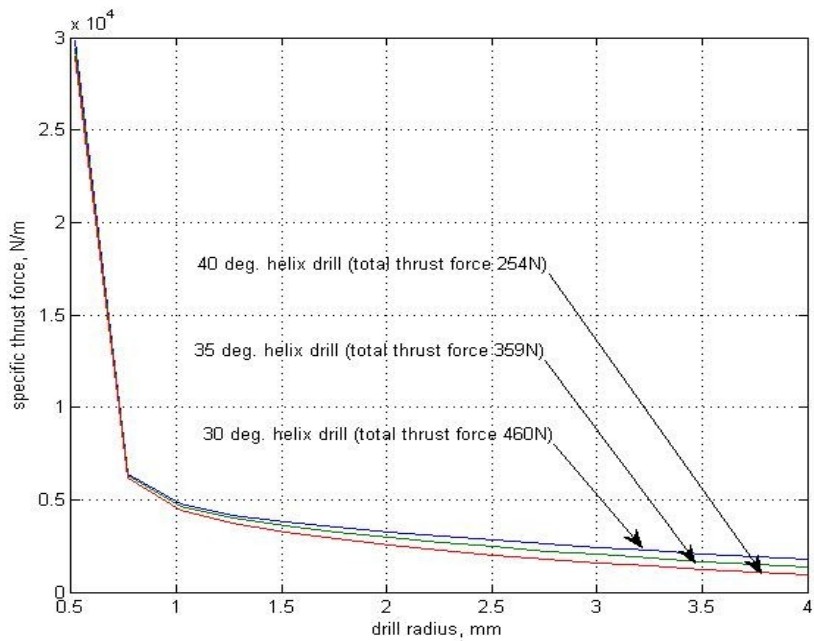


Figure 4.11. Predicted thrust forces for the standard 8mm twist drill with the 30°, 35° and 40° helix angles

An increase of the helix angle  $\delta$  leads to the decrease of both the thrust force and the torque as seen on Figure 4.11. and Figure 4.12.

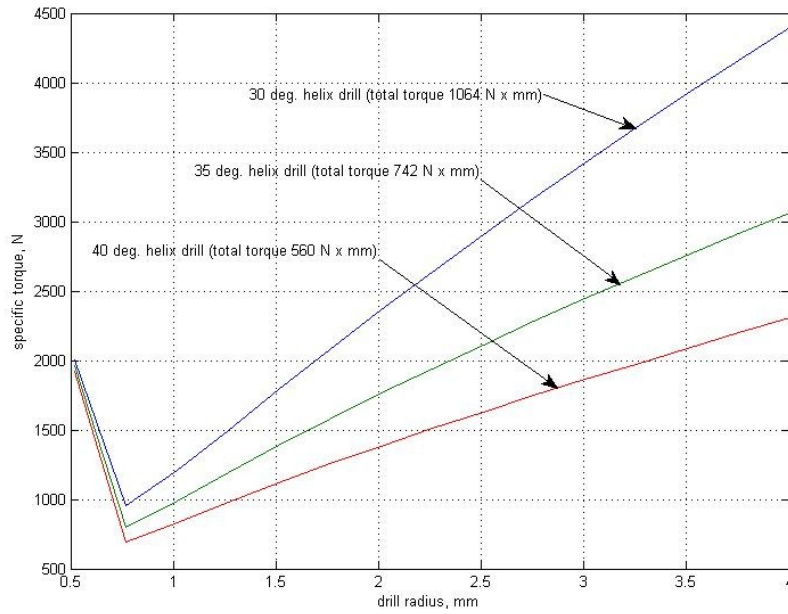


Figure 4.12. Predicted torques for the standard 8mm twist drill with the 30°, 35° and 40° helix angles

A decrease of the half-web thickness  $t_p$  leads to the decrease of both the thrust force and the torque as seen on Figure 4.13 and Figure 4.14.

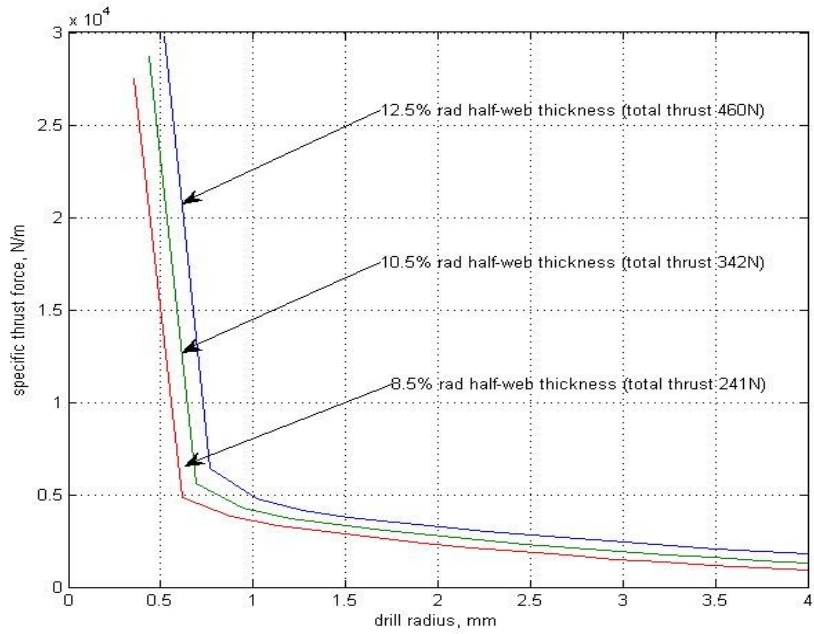


Figure 4.13. Predicted thrust forces for the standard 8mm twist drill with the half-web thickness represents 8.5%, 10.5% and 12.5% of the drill radius.

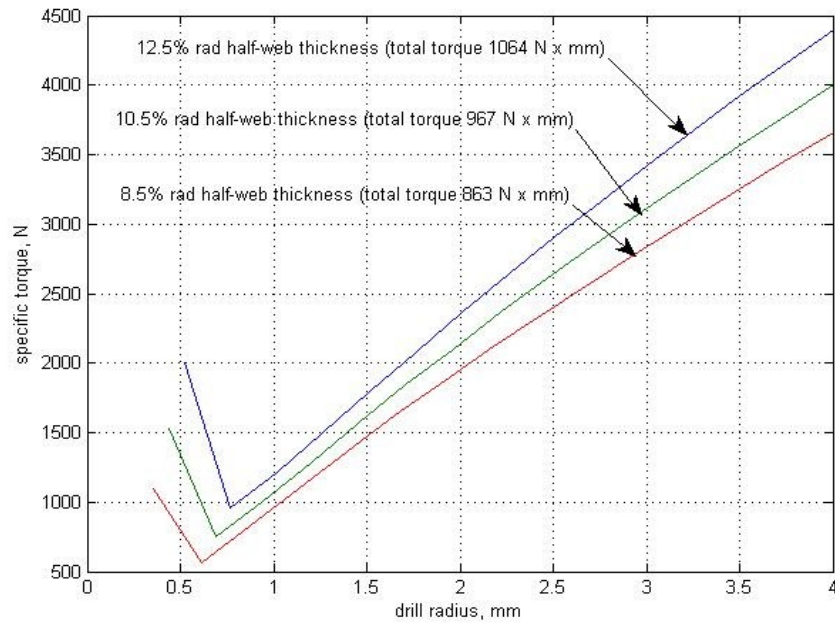


Figure 4.14. Predicted torques for the standard 8mm twist drill with the half-web thickness represents 8.5%, 10.5% and 12.5% of the drill radius.

The improved method, which was applied for the calculations of the thrust force and torque on the straight primary cutting edge may also be expanded to predicting the thrust forces and torque for the secondary cutting edge for the split point drills and for drills with variable half-web thickness, which are widely used in modern metal cutting. Moreover, the same technique can be applied for various types of inserted drills.

## Chapter 5. Summary and conclusions

The three existing methods were studied and analyzed. The improved method offers a perfected way for calculating the thrust and torque in high speed drilling. The thesis focused on the primary cutting edge, which is the main contributor of thrust force and torque. The geometrical analysis proved that it is not the feed angle but the reference angle that is the lead factor which affects the dynamic rake angle and thus the thrust force and torque. The new formulas for the calculation of thrust and torque have been derived and contain corrections of the previously suggested formulas of Chen and Elhachimi. The improved method presents the proper definitions of the dynamic rake angle and the uncut chip thickness, proves the negligibility of the feed angle and gives accurate representation of the elemental forces acting along the primary cutting edge, as well as the total thrust force and the torque. It allows to make calculations based on the basic geometrical features of the drill alone, as well as the cutting conditions and the properties of the machined material. This approach, unlike the other existing methods allows to exclude the empirically determined chip flow angle from both formulas for the calculations of the thrust and torque.

The Matlab program has been developed and comparisons between predictions and experimental results have been carried out and a satisfactory agreement has been achieved.

## References

1. Morse, S.A., 1863, "Improvements in drill bits", American Patent No:38
2. Merchant, M.E., 1954, "Basic mechanics of the metal cutting process", *Journal of Applied Mechanics*, pp. 168–175.
3. Boothroyd, G. and Knight, W.A., 2006, "Fundamentals of Machining and Machine Tools", Third Edition, Taylor and Francis.
4. Stephenson, D.A. and Agapiou, J.S., 1997, "Metal Cutting Theory and Practice", Marcel Dekker, New York.
5. Trent, E.M. and Wright, P.K., 2000, "Metal Cutting", 4th. Edition, Butterworth-Heinemann, Boston.
6. Altintas, Y., 2000, "Manufacturing Automation: Metal Cutting Mechanics, Machine Tool Vibrations, and CNC Design", Cambridge University Press, Cambridge.
7. Childs, T.H.C., Maekawa, K., Obikawa, T., Yamane, Y., 2000, "Metal Machining. Theory and Application", Arnold, London.
8. DeGarmo, E.P., Black, J.T., Kohser, R.A., 1997, "Materials and Processes in Manufacturing", Prentice Hall, Upper Saddle River, NJ.
9. Lee, E.H. and Shaffer, B.W., 1951, "The theory of plasticity applied to a problem of machining", *ASME Journal of Applied Mechanics*, Vol.18, pp 405-413.
10. Hill R., 1954, "The mechanism of machining: a new approach", *Journal of Mechanics and Physics of Solids*, Vol. 3, pp. 47-53.
11. Dewhurst, W., 1978, "On the non-uniqueness of the machining process", *Proceedings of the Royal Society, London, A*, Vol. 360, pp. 587-609.

12. Oxford Jr., C.J., 1955, "On the drilling of metals - I. Basic mechanics of the process", *Trans ASME*, Vol. 77, pp.103-114.
13. Bera, S.K. and Bhattacharyya, A., 1966, "Mechanics of drilling process", *Journal of Inst. Engineering (India) ME 6* Vol. 46 (11) pp. 265–276.
14. Williams, R.A., 1974, "A study of the drilling process", *Journal of Engineering for Industry*, pp. 1207–1215.
15. Mauch C.A. and Lauderbaugh L.K., 1990, "Modeling the drilling process - an analytical model to predict thrust force and torque", *Computer Modeling and Simulation of Manufacturing Processes*, ASME Prod. Eng. Div., Vol. 48, pp. 59–65.
16. Armarego E.J.A. and Wright J.D., 1984, "Predictive models for drilling thrust and torque - a comparison of three flank configurations", *Annals of the C.I.R.P.*, Vol. 33, pp. 5–10.
17. Armarego, E.J.A. and Cheng, C.Y., 1972, "Drilling with flat rake face and conventional twist drills – I. Theoretical investigation", *International Journal of Machine Tools and Manufacture*, Vol. 12, pp. 17–35.
18. Armarego, E.J.A. and Cheng, C.Y., 1972, "Drilling with flat rake face and conventional twist drills - II. Experimental investigation", *International Journal of Machine Tools and Manufacture*, Vol. 12, pp. 37–54.
19. Wiriycosol, S. and Armarego, E.J.A., 1979, "Thrust and torque prediction in drilling from a cutting mechanics approach", *Annals of the C.I.R.P.* Vol. 28(1), pp 87–91.

20. Armarego, E.J.A., 1997, "Material Removal Processes-Twist Drills and Drilling Operations", University of Melbourne, Australia.
21. Stephenson D.A. and Agapiou J.S., 1992, "Calculation of main cutting edge forces and torque for drills with arbitrary point geometries", International Journal of Machine Tools Design and Research, Vol. 32(4), pp. 521–538.
22. Chandrasekharan, V., Kapoor, S.G., DeVor, R.E., 1995, "A mechanistic approach to predicting cutting forces in drilling - with application to fiber reinforced composite materials", Transactions of the ASME, Journal of Engineering for Industry Vol. 117 (3), pp. 559–570.
23. Kachanov, L.M., 1971, "Foundations of the Theory of Plasticity", North Holland, Amsterdam.
24. Watson, A.R., 1985, "Drilling model for cutting lip and chisel edge and comparison of experimental and predicted results I - initial cutting lip model", International Journal of Machine Tool Design and Research Vol. 25(4), pp. 347–365.
25. Watson, A.R., 1985, "Drilling model for cutting lip and chisel edge and comparison of experimental and predicted results. II - reversed cutting lip model", International Journal of Machine Tool Design and Research Vol. 25(4), pp. 367–376.
26. Watson, A.R., 1985, "Drilling model for cutting lip and chisel edge and comparison of experimental and predicted results. III - drilling model for chisel edge", International Journal of Machine Tool Design and Research Vol. 25(4), pp. 377–392.

27. Watson, A.R., 1985, "Drilling model for cutting lip and chisel edge and comparison of experimental and predicted results. IV - drilling tests to determine chisel edge contribution to torque and thrust", *International Journal of Machine Tool Design and Research*, Vol. 25(4), pp. 393–404.
28. Rubenstein, C., 1991, "The torque and thrust force in twist drilling - I. Theory", *International Journal of Machine Tools and Manufacture*, Vol. 31, pp. 481–489.
29. Rubenstein, C., 1991, "The torque and thrust force in twist drilling - II. Comparison of experimental observations with deductions from theory", *International Journal of Machine Tools and Manufacture* Vol. 31, pp. 491–504.
30. Zhang, L.B., Wang, L.J., Liu, X.Y., Zhao, H.W., Wang, X., Lou, H.Y., 2001, "Mechanical model for predicting thrust and torque in vibration drilling fibre-reinforced composite materials, *International Journal of Machine Tools and Manufacture*, Vol. 41, pp. 641–657.
31. Wang, L.P., Wang, L.J., He, Y.H., Yang, Z.J., 1998, "Prediction and computer simulation of dynamic thrust and torque in vibration drilling", *Proceedings Institution of Mechanical Engineers Part B*, Vol. 212 (6), pp. 489–497.
32. Wang, L.P., Wang, J.S., Ye, P.Q., Wang, L.J., 2001, "A theoretical and experimental investigation of thrust and torque in vibration microdrilling", *Proceedings Institution of Mechanical Engineers Part B*, Vol.215, pp. 1539–1548.
33. Yang J.A., Jaganathan V., Du R., 2002, "A new dynamic model for drilling and reaming processes", *International Journal of Machine Tools and Manufacture*, Vol. 42, pp. 299–311.

34. Elhachimi, M., Torbaty, S., Joyot, P., 1999, "Mechanical modeling of high speed drilling: 1 predicting torque and thrust", *International Journal of Machine Tools and Manufacture*, Vol. 39, pp.553-568.
35. Elhachimi, M., Torbaty, S., Joyot, P., 1999, "Mechanical modeling of high speed drilling: 2 predicted and experimental results", *International Journal of Machine Tools and Manufacture*, Vol. 39, pp. 569-581.
36. Chen, W.C., Fuh, K.H., Wu, C.H., Chang, B.R., 1996, "Design optimization of a split-point drill by force analysis", *Journal of Materials Processing Technology*, Vol.58, Issues 2-3, pp. 314-322.
37. Kapoor, S. G., DeVor, R.E., Zhu, R., Gajjela, R., Parrakal, G. and Smithey, D., "Development of Mechanistic Models for the Prediction of Machining Performance: Model Building Methodology," *ASME Journal of Machining Science and Technology-An International Journal*, 2:2, 213-238, 1998.
38. Chandrasekharan, V., Kapoor, S.G., DeVor, R.E., 1998, "A Mechanistic Model to Predict the Cutting Force System for Arbitrary Drill Point Geometry," *ASME Journal of Manufacturing Science and Engineering*, Vol. 120 (3), pp. 563-570.
39. Ehmann, K. F., Kapoor, S.G., DeVor, R.E. and Lazoglu, I., 1997, "Machining Process Modeling; A Review," *ASME Journal of Manufacturing Science and Engineering*, Vol.119 (1), pp. 1-9.
40. Gong, Y., Ehmann, K.F., 2001, "Mechanistic model for dynamic forces in micro-drilling", *Proceedings of 2001 ASME International Mechanical Engineering Congress and Exposition*, Nov. 11–16, 2001, New York, NY.

41. Gong, Y., Cheng, L., Ehmann, K.F., 2005, "Dynamics of initial penetration in drilling: Part 1 - Mechanistic model for dynamic forces", *Journal of Manufacturing Science and Engineering, Transactions of the ASME*, Vol.127 (2), pp. 280-288.
42. Gong, Y., Cheng, L., Ehmann, K.F., 2005, "Dynamics of initial penetration in drilling: Part 2 - Motion models for drill skidding and wandering with experimental verification", *Journal of Manufacturing Science and Engineering, Transactions of the ASME*, Vol. 127 (2), pp. 289-297.
43. Fuh, K.H., 1987, "Computer Aided Design and Manufacturing of Multi-Facet Drills", PhD Dissertation, University of Wisconsin at Madison.
44. Guo, Y., Dornfeld, D.A., 1998, "Finite element analysis of drilling burr minimization with a backup material", *Transaction of the North American Manufacturing Research Institution of SME*, Vol. 26, pp. 207-212.
45. Min, S., Dornfeld, D.A., Kim, J., Shyu, B., 2000, "Finite element modeling of burr formation in metal cutting", *Machining Science and Technology*, Vol. 5, pp.307-322.
46. Shatla, M., Altan, T., 2000, "Analytical modeling of drilling and ball end milling", *Journal of Materials Processing Technology*, Vol. 98, pp. 125-133.
47. Bono, M., Ni, J., 2001, "The effects of thermal distortions on the diameter and cylindricity of dry drilled holes", *International Journal of Machine Tools and Manufacture*, Vol. 41, pp. 2261-2270.
48. Bono, M., Ni, J., 2002, "A model for predicting the heat flow into the workpiece in dry drilling", *Journal of Manufacturing Science and Engineering*, Vol. 124, 773-777.

49. Strenkowski, J. S., Hsieh, C. C., Shih A. J., 2004, "An analytical finite element technique for predicting thrust force and torque in drilling", *International Journal of Machine Tools and Manufacture*, Vol. 44 (12-13), pp. 1413-1421.
50. Zhao J., Liu Q., Lee K.W., Choa V., Teh C.I., Hinds B.K., Treanor G.M., 2000, "Analysis of stresses in micro-drills using the finite element method", *International Journal of Machine Tools and Manufacture*, Vol. 40 (10), pp. 1443-1456.
51. Astakhov, V.P., Osman, M.O.M., 1996, "Analytical evaluation of the cutting forces in self-piloting drilling using the model of shear zone with parallel boundaries. Part 1. Theory", *International Journal of Machine Tools and Manufacture*, Vol. 36, (11), pp. 1187-1200.
52. Astakhov, V.P., Osman, M.O.M., 1996, "Analytical evaluation of the cutting forces in self-piloting drilling using the model of shear zone with parallel boundaries. Part 2: Application", *International Journal of Machine Tools and Manufacture*, Vol. 36, (12), pp. 1335-1345.
53. Wang, L.J., Wang, X., Zhao, H.F., 2004, "Effect of the cutting ratio on cutting forces and the drill life in vibration drilling", *International Journal of Advanced Manufacturing Technology*, Vol. 24 (11-12), pp. 865-872.
54. Salama, S., El Sawy, A. H., 1996, "The dynamic geometry of a twist drill point" *Journal of Materials Processing Technology*, Vol. 56 (1-4), pp. 45-53.
55. Wang, J., Zhang, Q., 2008, "A study of high-performance plane rake faced twist drills. Part II: Predictive force models", *International Journal of Machine Tools and Manufacture*, Vol. 48 (11), pp. 1286-1295.

56. Wang, J., Zhang, Q., 2008, "A study of high-performance plane rake faced twist drills. Part I: geometrical analysis and experimental investigation", *International Journal of Machine Tools & Manufacture*, Vol. 48 (11), pp. 1276-1285.
57. Langella, L., Nele, A., Maio, A., 2005, "Torque and thrust prediction model for drilling of composite materials. Composites Part: A", *Applied Science and Manufacturing*, Vol. 36 (1), pp. 83-93.
58. Chang, S.S.F., Bone, G.M., 2009, "Thrust force model for vibration-assisted drilling of aluminum 6061-T6", *International Journal of Machine Tools and Manufacture*, Vol. 49 (14), pp. 1070-1076.
59. Roukema, J.C., Altintas, Y., 2007, "Generalized modeling of drilling vibrations. Part I: Time domain model of drilling kinematics, dynamics and hole formation" *International Journal of Machine Tools and Manufacture*, Vol. 47 (9), pp. 1455-1473.
60. Roukema, J.C., Altintas, Y., 2007, "Generalized modeling of drilling vibrations. Part II: Chatter stability in frequency domain", *International Journal of Machine Tools and Manufacture*, Vol. 47 (9), pp. 1474-1485.
61. Guibert, N., Paris, H., Rech, J., Claudin, C., 2009, "Identification of thrust force models for vibratory drilling", *International Journal of Machine Tools and Manufacture*, Vol. 49 (9), pp. 730-738.
62. Nagao, T., Hatamura, Y., Mitsuishi, M., 1994, "In-Process Prediction and Prevention of the Breakage of Small Diameter Drills Based on Theoretical Analysis", *Annals of the C.I.R.P - Manufacturing Technology*, Vol. 43 (1), pp. 85-88.

63. Hsieh, J.F., Lin, P.D., 2002, "Mathematical model of multiflute drill point", *International Journal of Machine Tools and Manufacture*, Vol. 42 (10), pp. 1181-1193.
64. Sahu, S.K., DeVor, R.E., Kapoor, S.G., 2004, "Modeling of forces for drills with chip-breaking grooves", *Transactions of the ASME, Journal of Manufacturing Science and Engineering*, Vol. 126 (3), pp. 555-564.
65. Arvajah, T., Ismail, F., 2006, "Machining stability in high-speed drilling-Part 1: Modeling vibration stability in bending", *International Journal of Machine Tools and Manufacture*, Vol. 46 (12-13), pp. 1563-1572.
66. Lotfi, B., Zhong, Z.W., Khoo, L.P., 2009, "Prediction of cutting forces along Pythagorean-hodograph curves", *International Journal of Advanced Manufacturing Technology*, Vol. 43 (9-10), pp. 872-882.
67. Lotfi, B., Zhong, Z.W., Khoo, L.P., 2009, "Variable feed rates and variable machine forces for a constant material removal rate and constant cutting force along Pythagorean-hodograph curves", *International Journal of Advanced Manufacturing Technology*, Vol. 40 (1-2), pp. 171-178.
68. Kessentini, A., Zghal, B., Karra, C., Louati, J., Haddar, M., 2006, "Simulation and modeling of the vibration effect on the hole form in drilling", *International Journal of Simulation Modeling*, Vol. 5 (4), pp. 133-144.
69. Abele, E., Fujara, M., 2010, "Simulation-based twist drill design and geometry optimization", *Annals of the C.I.R.P - Manufacturing Technology*, Vol. 59 (1), pp. 145-150.

70. Pirtini, M., Lazoglu, I., 2005, "Forces and hole quality in drilling", *International Journal of Machine Tools and Manufacture*, Vol. 45 (11), pp. 1271-1281.
71. Muthukrishna Selvam, S.V., Sujatha, C., 1995, "Twist drill deformation and optimum drill geometry", *Computers and Structures*, Vol. 57 (5), pp. 903-914.
72. Chen, W.C., 1997, "Applying the finite element method to drill design based on drill deformations", *Finite Elements in Analysis and Design*, Vol. 26 (1), pp. 57-81.
73. Audy, J., 2008, "A study of computer-assisted analysis of effects of drill geometry and surface coating on forces and power in drilling", *Journal of Materials Processing Technology*, Vol. 204 (1-3), pp. 130-138.
74. Hamade, R.F., Seif, C.Y., Ismail, F., 2006, "Extracting cutting force coefficients from drilling experiments." *International Journal of Machine Tools and Manufacture*, Vol. 46 (3-4), pp. 387-396.
75. Huang, H.T., 1994, "Prediction of thrust and torque for multifacet drills", *Transactions of the ASME, Journal of Engineering for Industry*, Vol. 116 (1), pp. 1-7.
76. Huang, H.T., 1994, "Analysis of clearance and rake angles along cutting edge for multifacet drills", *Transactions of the ASME, Journal of Engineering for Industry*, Vol. 116 (1), pp. 8-16.
77. Xiong, L., Fang, N., Shi, H., 2009, "A new methodology for designing a curve-edged twist drill with an arbitrarily given distribution of the cutting angles along the tool cutting edge", *International Journal of Machine Tools and Manufacture*, Vol. 49 (7-8), pp. 667-677.

78. Radzevich, S.P., 2007, "Kinematic Geometry of Surface Machining", CRC Press.
79. Oxley, P.L.B., 1989, "The Mechanics of Machining: An Analytical Approach to Assessing Machinability, Ellis Horwood, Chichester.
80. Mitsubishi Web General Catalog, Mitsubishi Materials Corporation,  
<http://www.mitsubishicarbide.com>
81. Production Machining, 2013, Gardner Business Media, Inc.